DEPARTAMENT OF CHEMISTRY

NOVA SCHOOL OF
SCIENCE & TECHNOLOGY

Daniela Borja da Cunha

BSc in Biochemistry

Green synthesized silver nanoparticles as non-invasive therapy for Cutaneous Leishmaniasis

MASTER IN BIOORGANIC CHEMISTRY

NOVA University Lisbon

September 2023

DEPARTAMENT OF CHEMISTRY

Green synthesized silver nanoparticles as non-invasive therapy for Cutaneous Leishmaniasis

Daniela Borja da Cunha

BSc in Biochemistry

Adviser: Dr. Sandra Isabel Dias Simões
Auxiliar Researcher, Faculdade de Farmácia, Universidade de Lisboa

Co-adviser: Dr. Manuela Colla Carvalheiro
Auxiliar Researcher, Faculdade de Farmácia, Universidade de Lisboa

Examination Committee:

Chair: Prof. Dr. Luísa Maria da Silva Pinto Ferreira,
Associate Professor with aggregation, FCT-NOVA

Rapporteurs: Prof. Dr. Ana Luísa Almaça da Cruz Fernando,
Associate Professor, FCT-NOVA

Adviser: Dr. Sandra Isabel Dias Simões
Auxiliar Researcher, Faculdade de Farmácia, Universidade de Lisboa

MASTER IN BIOORGANIC CHEMISTRY

NOVA University Lisbon
September 2023

Green synthesized silver nanoparticles as non-invasive therapy for Cutaneous Leishmaniasis

I dedicate this thesis to my parents and grandfather.

ACKNOWLEDGMENTS

First, I want to thank Dr. Manuela Colla Carvalheiro and Dr. Sandra Simões for accepting me in their laboratory and for their orientation. Through this time, I gained more knowledge and insight in the pharmaceutical area. I want also to thank Catarina for helping me improving my practical abilities in the cytotoxic studies and warning me for better laboratory practices. Your recommendations and guidance were crucial to my professional and personal growth.

For my laboratory colleagues, Jacinta, Pedro, Mariana, Marta, Patrícia and many others for helping me in the laboratory and for making work easier with their joy.

My family, especially my mother and father for their love and patience in stressful times. My aunts Arlete, Carmen, Uzia and Carina for their support. My uncle Paulo for giving me valuable lessons. My cousins, David, Jéssica and Vanessa for always cheering me up.

The friends that university gave to me, Alejandra and Catarina, for the companionship, laughs, tears, and joy that five years of university gave to us. I hope that we have more years to enjoy.

My friends, Nafina, Sara, Solange and Zahara for listening to all my daily complaints and, cheering me up and increasing my self-esteem.

My friends Luís and Kajó for always distracting me when life gets hard, their support and help.

For the least but one of my pillars, my childhood friends, Soraia, Sandra and Felícia for all these years of love and support. More years will come. Our friendship means the world to me.

“Do not confuse the reality you live in,

with the ideas you have in your head.” (Amílcar Cabral).

ABSTRACT

Silver nanoparticles (AgNP) are emerging as one of the fastest-growing nanomaterials owing to exceptional unique properties with numerous applications in different areas. Their biosynthesis employing phytochemicals of plant extracts as reducing and coating agents is a simple, efficient, and green method. Agro-food industries generate massive quantities of organic waste, a renewable source of biomolecules for AgNP biosynthesis. The main objective of this thesis was to prepare biogenic AgNP using a green tomato extract (TE) as reducing and stabilizing agent, obtained by subcritical water extraction (SWE). The effects of TE and $AgNO_3$ concentration, reaction time, pH, and temperature on AgNP synthesis, particle size and surface charge were investigated. AgNP were characterized by UV-Vis spectrophotometry, particle size, surface charge, microscopical analysis. *In vitro* cytotoxicity against human keratinocyte cell line HaCaT and macrophage-like cell line THP-1 was assessed. Antileishmanial activity was evaluated against *Leishmania major* promastigotes. Antimicrobial activity was determined in an *ex vivo* skin model and *in vitro* against Gram(-) and Gram(+) reference strains. The wound healing capability of AgNP was estimate in an incisional *in vivo* wound mouse model. The developed AgNP have a surface plasmon resonance (SPR) band between 402-406 nm, a size of ±60 nm, are negatively charged (-42 mV), spherical and disperse. A dose-response curve for THP-1 cell with no major toxicity was observed. The *in vitro* and *ex vivo* studies prove that AgNP do not compromise skin cells and can decrease cutaneous irritation. Gram(-) bacteria were more susceptible to AgNP. The AgNP formulated in a gel revealed similar wound healing properties as topical commercial silver-containing ointment. These AgNP inhibited the growth *L. major* promastigotes at concentrations safe for human cells and possess characteristics consistent with a nano drug-delivery system (size, shape) hence can become a promising tool for topical treatment of cutaneous leishmaniasis, a neglected tropical disease.

Keywords: Silver nanoparticles, nanoparticle biosynthesis, green tomato, green chemistry

RESUMO

As nanopartículas de prata (AgNP) emergiram como nanomaterial em rápido crescimento devido às suas propriedades únicas, com inúmeras aplicações em diferentes áreas. A sua biossíntese utilizando extratos vegetais como agentes redutores e de estabilização é um método simples, eficiente e ecológico. A indústria agro-alimentar gera grandes quantidades de resíduos orgânicos, constituindo uma fonte de moléculas para a biossíntese de AgNP. O objetivo principal desta tese foi a síntese biogénica de AgNP utilizando um extrato verde de tomate como agente redutor e estabilizante, obtido por extração com água subcrítica. Foram investigados os efeitos da concentração de extrato, $AgNO_3$, tempo de reação, pH e temperatura na síntese. Foram caracterizadas por espectrofotometria UV-Vis, tamanho de partícula, carga superficial e microscopia. Foi avaliada a citotoxicidade in vitro em queratinócitos humanos HaCaT e a macrófagos THP-1. A atividade antileishmania foi avaliada em promastigotas de *Leishmania major*. A atividade antimicrobiana foi determinada em modelo de pele *ex vivo* e *in vitro* contra estirpes de referência. Através de um modelo murino de ferida foi estimada a capacidade das AgNP na cicatrização de feridas. As AgNP desenvolvidas possuem uma banda SPR entre 402-406 nm, um tamanho de ± 60 nm, carga superficial negativa (-42 mV), são esféricas e dispersas. Não foi observada toxicidade em macrófagos THP-1. Os estudos *in vitro* e *ex vivo* comprovam que as AgNP não comprometem as células da pele e podem diminuir a irritação cutânea. As bactérias Gram (-) foram mais suscetíveis às AgNP. Quando formuladas em gel, as AgNP revelaram propriedades de cicatrização de feridas semelhantes às da pomada comercial. Estas AgNP inibiram o crescimento de promastigotas de *L. major* em concentrações seguras para células humanas e possuem características consistentes com um sistema de administração de nanofármacos, podendo tornar-se uma ferramenta promissora para o tratamento tópico da leishmaniose cutânea, uma doença tropical negligenciada.

Palavras-chave: Nanopartículas de prata, biossíntese de nanopartículas, tomate verde, química verde

CONTENTS

LIST OF FIGURES

LIST OF TABLES

LIST OF ABBREVIATIONS

DNA	Deoxyribonucleic Acid
PARP	Poly (ADP-Ribose) Polymerase
PEG	Polyethylene Glycol
EDTA	Ethylenediamine Tetraacetic Acid
TIAB	Titanium-Argentum-Bezoicum
SOD	Superoxide Dismutase
LPG	Lipophosphoglycan
MTT	3-(4,5-dimethylthiazol-2-yl)-2,5-diphenyl tetrazolium bromide
MTS	3-[4,5,dimethylthiazol-2-yl]-5-[3-carboxymethoxy-phenyl]-2-[4- sulfophenyl]-2H-tetrazolium
ANOVA	Analysis of variance

LIST OF ACRONYMS

AgNP	Silver Nanoparticles
ROS	Reactive Oxygen Species
RNS	Reactive Nitrogen Species
SWE	Subcritical Water Extraction
CL	Cutaneous Leishmaniasis
NTD	Neglected Tropical Disease
WHO	World Health Organization
OW	Old World
NW	New World
TE	Tomato Extract
iNOS	Inducible Nitric Oxide Synthase
DMEM	Dulbecco's modified Eagle's medium
RPMI	Roswell Park Memorial Institute Medium
AFM	Atomic Force Microscopy
TEM	Transmission Electron Microscopy
iFBS	Inactivated Fetal Bovine Serum
MIC	Minimal Inhibitory Concentration
TSA	Tryptic Soy Agar
SPR	Surface Plasmon Resonance
PdI	Polydispersity Index

LIST OF SYMBOLS

d(H) Hydrodynamic diameter

k Boltzmann's constant

T Absolute temperature

D Translational diffusion movement

η Viscosity

$\boldsymbol{U_E}$ Electrophoretic mobility

ε Dielectric constant

ζ Zeta potential

f(Ka) Henry's equation

1

INTRODUCTION

1.1 Silver nanoparticles

Historically, silver salts have been used to prevent the growth of microorganisms. They are still used in burns, cuts, wounds, and catheters to suppress infections [1,2]. Silver nanoparticles (AgNP), normally ranging between 1 and 100 nm in size, is a nanomaterial produced using nanotechnology that contains silver (Ag) atoms. It has a widespread presence in different consumer products due to AgNP strong bactericidal properties, and broad-spectrum antimicrobial activity [3].

The biological effects of AgNP are enhanced due to their high surface to volume ratio. Their small size also optimizes the electrical conductivity as well their thermal and optical activity [4]. There is no scientific consensus on how this nanoparticles work, but silver nanoparticles release Ag^+ ions more efficiently that non-particulated silver due of their greater surface area. Silver nanoparticles with 10 nm are proven to be detectable in the deepest layers of stratum corneum and could disperse and eliminate parasites [5]. Ag^+ can change the permeability of cell walls by attaching negatively to the charged cell wall. This effect of Ag^+ is possible due to its high reactivity and ionization [6]. Silver ions can directly interact with parasite surface, consequently, parasite membrane loose integrity and fluidity, conducting to apoptosis [7]. Additionally, AgNP can break the electron transport chain, interfering with the metabolism and ATP synthesis [8]. Besides, they stimulate the macrophages to release ROS, RNS and inflammatory cytokines that increases microorganism clearance [6]. Host cells generate substantial amounts of ROS when exposed to AgNP. Several proteins protect against ROS, one of which is glutathione, which scavenge ROS [9]. If this ability is lost, oxidative stress can lead to DNA damage, mitochondrial disruption and lipid and protein peroxidation [10]. Increased levels of ROS trigger the suppression of protein kinase B, leading to the overexpression of pro-apoptotic p38. Downregulation of the DNA repair enzyme PARP stimulates the expression of p53, which initiates the apoptotic process [11]. **Figure 1.1** summarizes the main properties of AgNP.

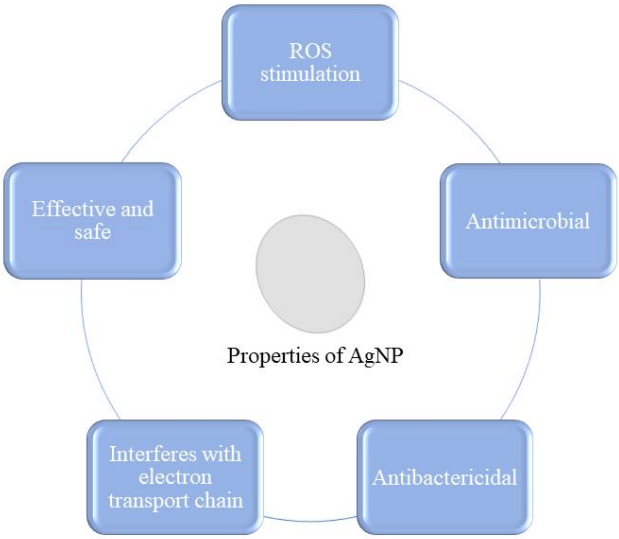

Figure 1.1. Medicinal effects of silver nanoparticles.

1.2 Synthesis of silver nanoparticles

The production of silver nanoparticles can be made by the "bottom-up" or the "top-down" methods. In top-down method, a bulk material is fractioned by milling or cutting to manufacture nanoparticles. Only physical methods are inserted in this category. Mechanical milling/ball milling, thermal composition, lithography, or laser ablation are standard physical methods to produce nanoparticles [12]. The synthesis is fast, doesn't employ radiation or dangerous solvents as reducing agents. The use of energy/heat is expensive and doesn't comply with the 6th rule of the green chemistry. An uneven distribution, low yield and solvent contamination can also occur [13]. In cases of chemical or biological synthesis, nanoparticles are manufactured by bottom-up method. In this procedure, molecules or atoms are mobilized to form nanoparticles. In chemical methods, silver nitrate is reduced by different inorganic groups. The silver ions are reduced to metallic silver, causing accumulation. Reducing solvents such as polyethylene glycol-block copolymers, ascorbate or sodium citrate are used for this purpose [13]. To stabilize the newly form nanoparticles, more solvents such trisodium citrate and sodium borohydride are applied [14]. Disadvantages are the control of size and of nanoparticle agglomeration that requires more procedures. The harmful and excessive use of solvents breaks the 3rd and 5th rules of green chemistry [4].

1.2.1 Biogenic synthesis

In recent years, the biogenic synthesis of AgNP mediated by biological systems including bacteria, fungi and plants has emerged as an environmentally friendly alternative. Plant extracts can be used to reduce the Ag^+ ions and form the nanoparticles. During this process, ions are reduced, followed by growth/nucleation and stabilization. Plants can do this by two ways: bioabsorption and bioreduction. In bioabsorption, plants absorb silver ions from water or soil. These plants have modified cell wall or peptides capable of binding metal ions, creating nanoparticles in the form of stable complexes. In bioreduction, the process is eased by bioreducing molecules such as flavonoids, enzymes, proteins, terpenoids, amino acids, carbohydrates, or vitamins [15]. Functional groups such as hydroxyl, carboxyl, and amino groups function as reducing agents. [16].

Extracts derived from agricultural waste, are also being used to form nanoparticles [17,18]. **Figure 1.2** represents one of such cases: green tomato discarded in substantial amounts by processing food industry is rich in several compounds that can function as silver reducing agents. Leaves, roots, fruits, flowers, or stems are usually dried to avoid spoilage but can also be frozen. The plant extracts are then added to an aqueous solution of silver salt (usually silver nitrate) [19]. Plant extracts can reduce Ag^+ extremely fast and efficiently; reaction can occur in fast as eleven min at 95 ºC [20]. This procedure is straightforward and can easily be scaled for industrial purposes. Nanoparticle size can be easily controlled by modulating the temperature, pH, stirring, silver nitrate concentration and plant extract concentration. Plant extracts produce stable nanoparticles with high antimicrobial and antioxidant properties [21]. In conventional methods, nanoparticles are coated with PEG, EDTA or polyvinyl alcohol to manage the oxidation and aggregation. In the biogenic method there is no need of a coating procedure as nanoparticles are coated with organic groups from plants, like amino acids or peptides [22]. The biosynthesis of AgNP allows thus to comply with various rules of green chemistry: reduced use of solvents and toxic solvents, minimization of energy used in the reaction, use of renewable raw materials, safer synthesis, and prevention of waste generation.

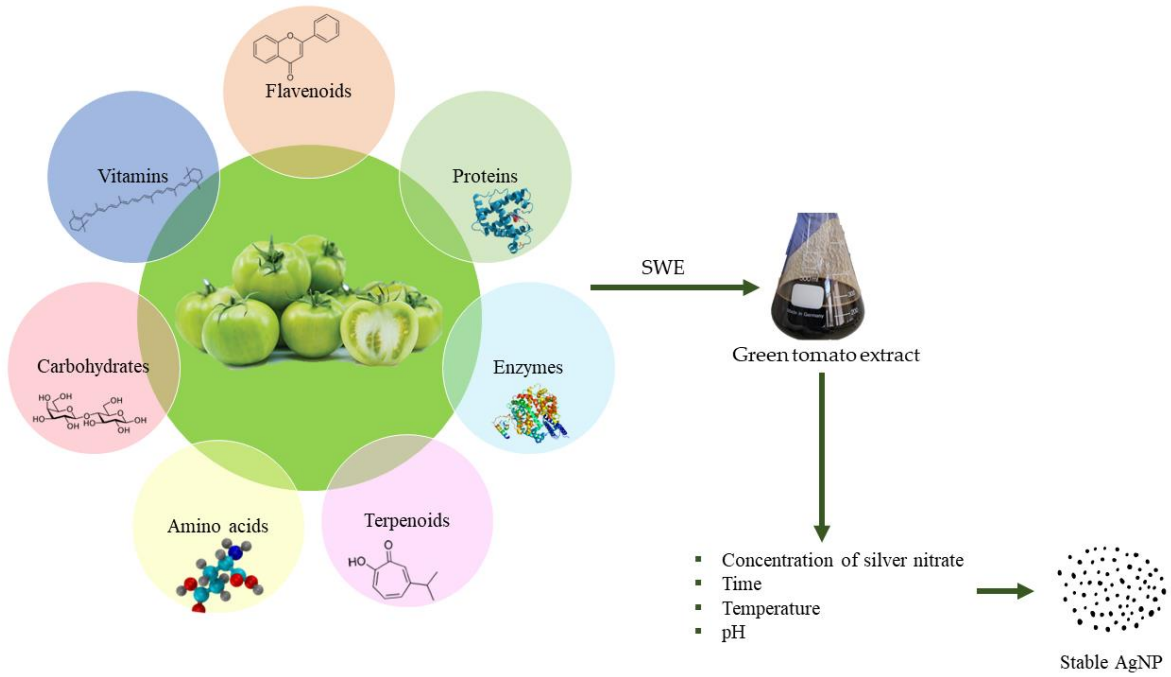

Figure 1.2. Biosynthesis of silver nanoparticles using green tomato extract. Extracts can be obtained from the fruit through several procedures, including ecofriendly techniques like subcritical water extraction (SWE).

1.2.2 Green tomato: a devalued fruit with differentiated potential in the synthesis of silver nanoparticles

Green tomato is a subproduct of the agro-food industry that has no economic value, despite the pharmacological, nutritional and health properties already reported [23]. Green tomatoes are rich in phenolic content, especially in β-carotene, phytoene and lycopene that are found in greater quantity when the tomato is mature. Green tomato is also rich in flavonoids, flavanones, and flavones, relating to antioxidant, anticancer, anti-inflammatory, and anti-viral characteristics [24]. Its consumption decreases LDL cholesterol and triglycerides, preventing respiratory and cardiovascular diseases, blindness, and some cancers [25–27]. The liver also benefits from tomato since it contains sulfur and chlorine, responsible for the detoxification of the liver, preventing cirrhosis [28]. The fruit is also rich in glycoalkaloids, especially α-tomatine, a versatile compound with numerous abilities: prevention from numerous cancer cells [29], antibiotic properties against pathogens [30,31] and reduction of cholesterol [32]. Other pharmacological activities have been reported: shields from muscle atrophy and increases muscles capacity and robustness [33] and has hemolytic action against red blood cells [34]. A mixture of salt and green tomatoes is used in some African communities to treat mouth issues like tooth decay, blisters, oral thrush, and ulcers, proving the fruit efficacy [35]. Chlorophyll is also good to eliminate body and mouth odor [36] and is used as a photo sensitizer as a therapy for cancer [37]. Green tomatoes are not so investigated as red tomatoes but could unleash new food and medicinal innovations.

1.3 Silver nanoparticles applications

Nanomedicine is one of the main fields that uses silver nanoparticles due to their antimicrobial and antiviral properties (**Figure 1.1**). Nanosilver-containing wound dressings have successfully avoid infection in necrotic tissues, reducing more than 50% of the colonies [38]. The complex TIAB is a titanium oxide carrier that incorporates active silver ions that can bind to other substances, increasing the ability to destroy microorganisms. The binding of TIAB with benzalkonium chloride, a biocide, is a popular combination of protection against different type of bacterial, viral, parasitic, and fungal infections [39]. The TIAB complex is used in dentistry as a dental disinfectant and topical medication and in gynecology as vaginal capsules and wound healing foams [40–43]. AgNP are also a valued resource for bone healing, since diseases that affect bones require transplants or invasive procedures. These treatments have a critical after care due to susceptibility for infections that can lead to loss of the bone or elevated inflammation [44]. AgNP improved bone tissue mineralization by stimulating MC3T3-1 pre-osteoblast cells [45]. Fluorescent AgNP are also popular for diagnosis, especially in cancer. These nanocarriers have high fluorescent characteristics that can be applied in fluorescent labeling [46], bioimaging [47], chemical sensing [48] and single-molecule microscopy [49]. These types of nanoparticles are very versatile having significant contributions in other areas. In water treatment, AgNP is replacing chlorine to disinfect water since chlorine can became dangerous when reacts with organic matter [50–52]. Increases the mean life of food when included in food packaging [53] and prevents odors and bacterial contamination in clothing [54].

1.3.1 Silver nanoparticles as a strategy for the treatment of Cutaneous Leishmaniasis

Cutaneous Leishmaniasis (CL) is a poverty-associated disease caused by *Leishmania* parasites and considered the most serious skin infection in many developing countries.

The increasing drug resistance of *Leishmania* parasites has demanded the research for new type of therapies. Biosynthesized nanoparticles [55] or nanoparticles combined with other molecules like chitosan [56] are being studied for their anti-parasitic abilities with recognized safety advantages [57]. Numerous examples of biosynthesis using different plant extracts, such as ginger rhizome, herbal leaf or artemisia have been described to manage *Leishmania* infections [58–60]. In the previous cited studies, the artemisia biogenic AgNP stimulated wound healing and augmented the rate of epithelialization *in vivo*, using BALB/c mice. These phenomena are attributed to flavonoids that are the main precursors in the biosynthesis. In herbal leaf AgNP, there is biocompatibility to macrophage, showing extremely low toxicity levels in MTT assays. In both ginger and herbal leaf biosynthesized AgNP, proved to be

active against amastigotes. These results show that infected macrophages are much more affected than uninfected ones, bringing hopeful prospects for new treatments of CL.

1.3.1.1 Geographic distribution of Cutaneous Leishmaniasis

Global warming and immigration have led to the spread of CL, a neglected tropical disease (NTDs), to other continents. According to the WHO, seventy animal species can be sources of transmission [61]. Surveillance centers suggest that dogs and rodents can be the main reservoirs of the disease [62][63]. Around 15-20 species of *Leishmania spp.* are known cause disease in humans worldwide, but only *Leishmania infantum* and *L. tropica* are endemic in Europe [64]. The species of *Leishmania* that cause CL can be divided (**Figure 1.3**) by the areas they occur: Old World (OW) CL is caused by the species endemic in Southern Europe, Asia and Africa, and New World (NW) CL is caused by the species existent in the South-Central Texas, Central and South America (except Chile and Uruguay) [65,66].

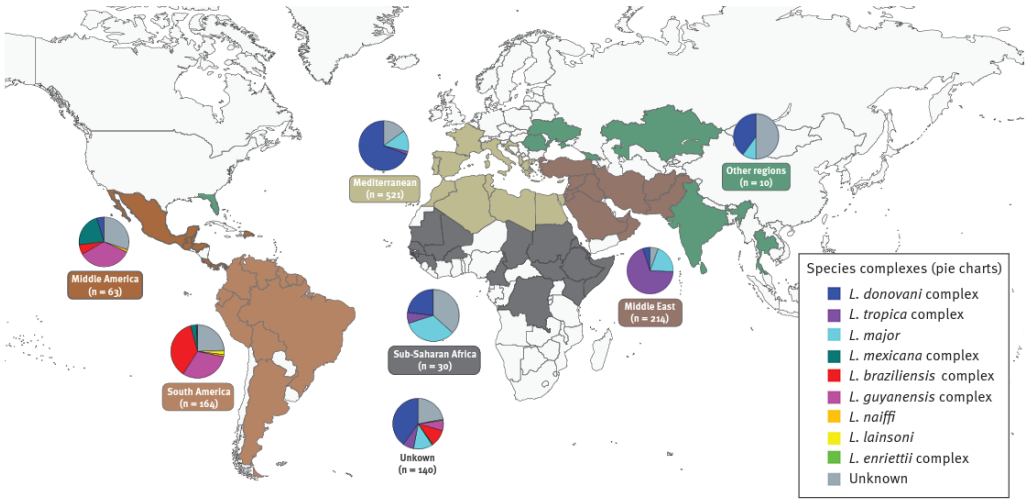

Figure 1.3. Endemic countries with CL. Reproduced from reference [64].

Most CL cases in Europe come from overseas. From 2012 until 2019, about 44% of OWCL cases originate from Syria, Afghanistan, the Middle East, and Pakistan, as migrants from these regions fled conflicts and humanitarian crises. Cases from Tunisia, Morocco and Algeria accounted for 34%, most of which were caused by visiting relatives or friends. As for the tourists, 8% were infected in Israel. Regarding to NWCL cases, more than half were among travelers infected in South America. Cases from Belize and French Guiana were military, accounting for 22% of cases. Ecuador accounts for about 7% of cases. The majority of domestic *L. infantum* cases in Europe originate from Southern Europe and the Balkans, especially Spain, which accounted for 60% of local cases due to holiday prevalence [64].

1.3.1.2 Life cycle of Cutaneous Leishmaniasis

The disease cycle begins with inoculation of *Leishmania* into the skin by the bite of female phlebotomine sandfly [67]. Sandflies have a molecule in their salivary glands that destroys neutrophils, the first defense line that is encountered [68]. At this stage, the flagellated promastigote form is inserted [69]. Parasites are recognized and targeted by the macrophages. Macrophages, present in the tissues, are responsible for the elimination of intracellular pathogens. This action proceeds by a process of phagocytosis (**Figure 1.4**) [70].

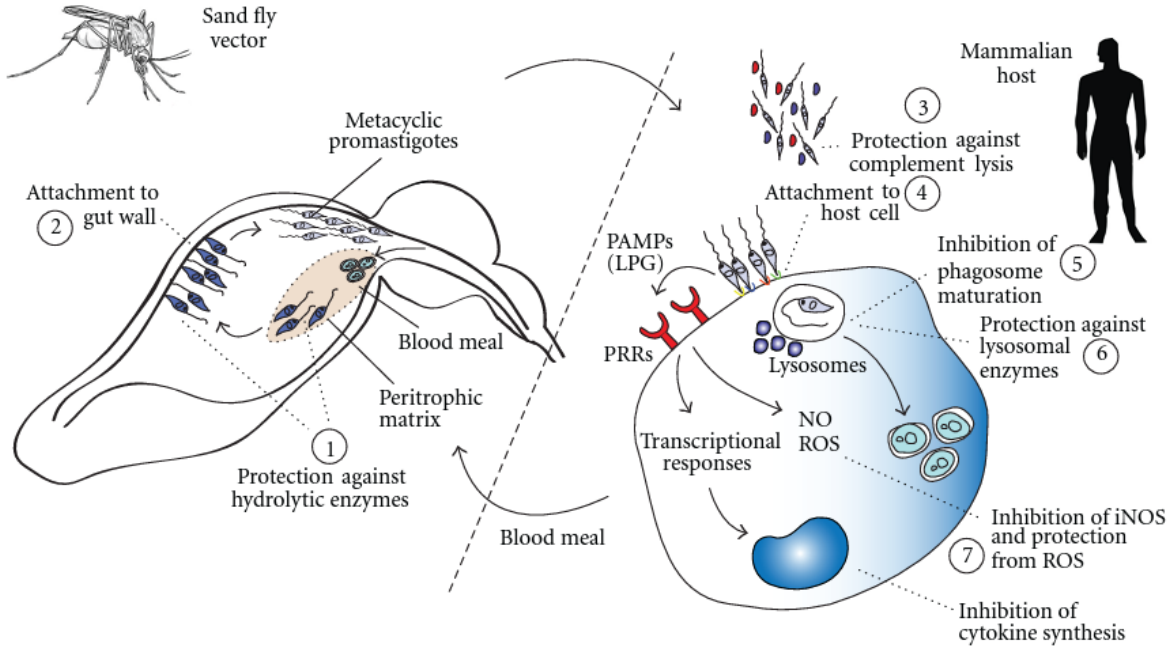

Figure 1.4. Different protection mechanisms from *Leishmania* against the macrophage response. Reproduced from reference [70].

Leishmania exploits the macrophage defense line with an eloquent strategy. Initially, in an environment with low pH and lytic cells, the parasite is surrounded in a phago-lysosome organelle inside of macrophage (**Figure 1.4**). There are two enzymatic complexes responsible to produce reactive species. NADPH oxidase 2 generates superoxide (O_{2}^{-}) and inducible nitric oxide synthase (iNOS) generates nitric oxide (NO^{-}). Inflammasome NLRP3 also stimulates the production of ROS and RNS, to kill the intruder [71]. *Leishmania* counterattacks this process with a thick lipophosphoglycan (LPG) coat that protects from adverse conditions imposed [70]. Protozoans interfere with the production of reactive species. The inflammasome activation is arrested by deubiquitination of protein A20, which is behind the maturation of IL-1β [72]. While the LPG protects the parasite, it stops the production of O_{2}^{-}, preventing the association of NOX2 at the surface of phago-lysosome [73]. Macrophages are then induced to generate arginase. This enzyme is in charge to create essential metabolites for the parasite, such as urea and L-ornithine. It decreases the formation of NO^{-}, as the metabolism of arginine, an

important molecule for the synthesis of this reactive specie, arises [74]. There is a production of superoxidase dismutase (SOD) homologues that neutralizes the reactive species. Furthermore, peroxynitrate ($ONOO^-$) derived from nitric oxide, is also neutralized by the peroxidases generated by the parasite [72]. In this phase, the amastigote form is multiplied. Incubation time is variable and can be days or months. The illness causes skin ulcers between 3-4 cm of diameter with central indentation and raised edges. If left untreated, CL can progress to diffuse leishmaniasis and mucosal leishmaniasis [63].

1.3.1.3 Available treatment and their limitations

The main goal of current CL management is to minimize the scars appearance, accelerate the treatment time and reduce the chance of relapse. The therapy is based on a strict number of chemotherapeutic agents. Pentavalent antimonials are the first-line treatment in developing countries considering the affordable price. The use of this therapy has been decreasing due to extensive duration, the pain involved, toxic side effects and increased drug resistance [75,76]. Other drugs such as paromomycin and miltefosine are used as second-line treatment. However, each drug has its own limitations, such as variable efficacy, low bioavailability, toxicity, and extensive treatment duration leading to patient withdrawal, or emergence of resistance [77]. Miltefosine, the only recognized oral agent with potential to treat leishmaniasis, presents severe signs of toxicity (e.g. teratogenicity) and induces parasite resistance which severely hampers its widespread use in the clinic [78,79]. Intravenous administration is avoided when skin lesions are small due to previous reasons. Amphotericin B is the most efficient drug that had major improvement in the side effects when using lipidic nanocarriers. Liposomal amphotericin B (AmBisome) is currently the most effective treatment available. The widespread use in endemic countries is hindered by the prohibitive cost [80]. These unsatisfactory treatments show that chemotherapy of leishmaniasis remains a challenge and there is an urgent need of new therapies [81]. The main advantage of using silver is the various mechanisms by which interacts with *Leishmania*. By delivering the drug in the skin lesions of CL, the drug acts directly in the parasite, reducing the dose and consequently, the toxic side effects [63].

Table 1.1 summarizes the mechanism of action of drugs clinically used to treat CL and the respective limitations.

Table 1.1. Mechanism of action of anti-leishmania drugs and their limitations.

Drug	Mechanism of action	Limitations	Ref.
Pentavalent antimonials	Pentavalent antimony (SbV) is converted in the active form trivalent antimony (SbIII) that decreases trypanothione synthesis by targeting trypanothione reductase (TR). The parasite becomes more prone to oxidative stress.	Prominent levels of SbV increase the multidrug resistance-associated protein 1 (MDRP1), augmenting drug efflux. There are also other efflux transporters involved such as ABCG2 and ARM56/ARM58.	[82–87]
Amphotericin B (AmB) and lipidic formulations	AmB has an amphipathic structure with affinity to form complexes with 24-subtituted sterols such as ergosterol and episterol that are very prominent in parasite's plasma membrane. The hydrophobic part engages with the membrane lipid while the hydrophilic part generates pores in the membrane. The pores will cause cell death due to the withdrawal of water, biomolecules, and cations.	Parasite membrane with low ergosterol has lower affinity with AmB. Some resistant species of *Leishmania* has efflux of AmB due to overexpression of MDR1 efflux pump. These strains also have higher oxidative stress tolerance.	[88–90]
Paromomycin	Paromomycin affects the mitochondrial membrane potential and consequently the respiration. Since the energy of the cell is affected, the flux of biomolecules is restrained and could lead to cell death. Paromomycin also destabilizes the dissociation of mitochondrial and cytoplasmatic ribosomes and reduces translation.	Although topical paromomycin can have comparable results to SbV in treating CL, *in vivo* and *in vitro* studies show that *Leishmania* can rapidly become resistant to paromomycin. The resistant strains show low affinity and binding to the drug, elevated tolerance to nitrosative stress and increased drug efflux due to overexpression of ABC transporters.	[91–95]
Miltefosine	Miltefosine targets the CDP-choline pathway of the parasite, destabilizing CTP-phosphocholinecytidylyltransferase function and affecting the regulation of phosphatidylcholine on the membrane. The compound could also target cytochrome C oxidase due to the decreased ATP levels of the parasites and mitochondria depolarization. The homeostasis of Ca^{2+} is disturbed by the stimulation of plasma membrane Ca^{2+} channels. These two targets can trigger apoptosis-like cell death. Some studies show that the drug can be responsible for the overexpression of IFN-γ receptor, augmenting the production of IFN-γ, IL-12, and TNF-a. This phenomenon increases the pro-inflammatory effect to the parasite due to the elevated sensibility of the macrophages to IFN-γ.	Mutations on genes ROS3 and MT that encodes for a transporter complex, involved in the absorption of miltefosine on the parasite.	[96–100]

1.4 Alternative strategies to treat Cutaneous Leishmaniasis

The development of nanotechnology and drug delivery systems is bringing novel approaches to decrease the toxicity of drugs used in CL management and improve their specificity to the target [101–103]. Macrophages have natural affinity for nanoparticulated systems which constitute an advantage of drug nanoencapsulation [104]. As an example, Amphotericin B is already commercialized incorporated in liposomes and in lipid complex [105].

Trifluralin derivatives are also alternative drug candidates that have been explored. The toxicity is low for mammals, but their low water solubility and easy sublimation were an obstacle for their pharmaceutical development [106,107]. In vitro tests of liposomal trifluralin derivatives showed satisfactory results that remain to be confirmed *in vivo* [108–110].

The **aim** of this thesis is to develop a method for the biogenic synthesis of silver nanoparticles using tomato extract as the reducing agent. Specific goals include:

- ✓ Task 1 - Biosynthesis and characterization of silver nanoparticles using tomato extract
- ✓ Task 2 - Evaluation of antioxidant activity of both extract and silver nanoparticles
- ✓ Task 3 - Biosafety evaluation of silver nanoparticles
- ✓ Task 4 – Assessment of *in vitro* antileishmanial activities of silver nanoparticles
- ✓ Task 5 – Antimicrobial activity assessment using an *ex vivo* activities
- ✓ Task 6 – Evaluation of therapeutic potential of developed nanoparticles using an *in vivo* wound healing model

Thesis outline:

I. Introduction
   A. Silver Nanoparticles medicinal features and synthesis methods
   B. General and Cutaneous Leishmaniasis applications of silver nanoparticles
   C. Cutaneous Leishmaniasis: cycle and geographical impact
   D. Treatments and alternatives for Cutaneous Leishmaniasis

II. Methods
   A. Materials
   B. Synthesis of biogenic silver nanoparticles made from green tomato extract: Pre-formulations and general procedure
   C. Chemical and physicochemical characteristics of the biogenic silver nanoparticles
   D. Biological assays to assess their properties

III. Discussion and results
   A. Chemical differences between green tomato extract obtained by two different methods
   B. Study of the variables impacting the characteristics of biogenic silver nanoparticles

C. Characteristics of the biogenic silver nanoparticles

D. Assessment of their properties through the biological tests

IV. Conclusions

A. The biogenic silver nanoparticles have pharmacological impact

V. Future work

A. Further studies that could improve the biogenic silver nanoparticles properties

2

METHODS

2.1 Materials

The green tomatoes were gently supplied by Italagro - Indústria de Transformação de Produtos Alimentares, S.A. Invitrogen Life Technologies (USA) was the supplier for both Dulbecco's modified Eagle's medium (DMEM) and RPMI (Roswell Park Memorial Institute Medium) 1640 media. Sigma–Aldrich (Spain) supplied silver nitrate ($AgNO_3$), dimethyl sulfoxide (DMSO) and 3-(4,5-dimethylthiazol-2-yl)-2,5-diphenyl tetrazolium bromide (MTT). Lecigel™ (sodium acrylates copolymer and lecithin) and Dermosoft® OMP (methylpropanediol, caprylyl glycol and phenylpropanol) were provided from Dr. Straetmans (Hamburg, Germany). All other chemical materials were of analytical grade and were used without any further purification. All solutions were freshly prepared using ultrapure water obtained in a MILLI-Q System Elix®3 from Millipore® by reverse osmosis process.

2.2 Methods

2.2.1 Green tomato extract preparation

Green tomatoes were cut in small pieces and blended in a mixer. Subcritical water treatment was performed using 600 g of tomatoes and around 60 mL of water at 190 ºC, 15 min of residence time and at a pressure of 50 bar in a batch high pressure reactor from Parr (model 4547, Illinois, USA). The extract obtained was filtered through a Whatman No. 1 filter paper and centrifuged at 1500 rpm for 10 min at room temperature (Sorvall RC6, Thermo Scientific, Waltham, MA). Extracts were stored in a refrigerator at 4 ^{o}C until use.

2.2.2 Green tomato extract characterization

2.2.2.1 Total carbohydrates content

Total carbohydrates content of the green tomato extract was determined by the phenol-sulfuric acid colorimetric method, using D(+)-glucose monohydrate as the standard. The phenol sulfuric method is a simple and reliable mechanism for the hydrolysis polysaccharides, oligosaccharides, and disaccharides into monosaccharides. Then, the reaction product reacts with phenol and shows a yellow-gold color. The samples are rich in hexose; therefore, glucose is used as a standard to construct the standard curve.

A stock solution of D(+)-glucose at 1 g/L was prepared and diluted for concentrations of 0.1 g/L, 0.075 g/L, 0.05 g/L, 0.025 g/L, 0.01 g /L and 0.005 g/L. Water was used as blank.

To 500 µL of either the standard solution or the extract, 1.5 mL of H_2SO_4 (96%) and 300 µL of a 5 % (w/v) aqueous solution of phenol were added. The resulting mixtures were stirred and incubated at 90 °C for 5 min in a dry bath. After cooling in a water bath, absorbances were measured at 490 nm and the results expressed as mg of glucose equivalents/mL [111].

2.2.2.2 Total Phenolic content

Total phenolic content of the green tomato extract was determined by the Folin-Ciocalteau method [112], using gallic acid (GA) as the standard. A stock solution of gallic acid at 1 g/L was made and diluted for solutions at 0.750 g/L, 0.5 g/L, 0.250 g/L, 0.100 g/L, 0.050 g/L, 0.025 g/L e 0.000 g/L. Before phenolics determination, a step of protein precipitation was performed, as protein interfere in phenolics quantification, adding 120 µL of 100 % (w/v) trichloroacetic acid to 800 µL of sample, stirring the mixture and stored it at -20 °C for 5 min, and then at 4 °C for 15 min. The mixture was then centrifuged at 12000 rpm for 15 min, and the precipitate was discarded.

For the phenolics quantification, to 20 µL of either recovered supernatant or standard gallic acid solutions, 1.58 mL of miliQ water and 100 µL of Folin-Ciocalteau reagent were added. The mixtures were stirred and incubated for 5 min at room temperature. Following this step, 300 µL of a saturated sodium carbonate solution was added and incubated at 40 ºC in a dry bath for 30 min. The absorbance was measured at 750 nm and results expressed as mg of GA equivalents/mL [111].

2.2.3 Silver nanoparticle synthesis

Silver nanoparticles were synthesized via the bio-reduction of silver ions mediated by biomolecules present in the tomato extract acting both as reducing and stabilizing agents. In the present work a solution of silver nitrate salt ($AgNO_3$) in ultrapure water was used as the silver source.

2.2.3.1 Determination of critical parameters

The unique chemical composition of the extract affects the characteristics and properties of the AgNP. The parameters examined included pH, $AgNO_3$ concentration, extract concentration, reaction time, and temperature.

2.2.3.1.1 96-well microplate experiment

In the first set of preliminary experiments the synthesis was carried out in 96-well microplates. Sixteen different conditions were tested in triplicate according to **Table 2.1**. The reaction was allowed to take place for 2.5 h at room temperature in the absence of light. The formation of the AgNP was monitored on a UV-VIS spectrophotometer. Conditions that showed a color change were subjected to further analysis.

Table 2.1. Reaction parameters tested in the 96-well microplate assay.

Reaction	TE (%) (v/v)	[$AgNO_3$] (mM)	pH
1	5	1	9
2	5	5	9
3	5	10	9
4	5	20	9
5	5	30	9
6	11	16	11
7	5	5	9
8	5	10	9
9	2.5	5	9
10	10	5	9
11	0.5	1	11
12	0.5	5	11
13	0.5	10	11
14	0.5	20	11
15	0.5	30	11
16	2.5	5	11
17	10	10	11
18	2.5	5	11
19	10	5	11
20	16.5	5	11

2.2.3.1.2 24-well microplate experiment

The second set of preliminary experiments was carried out in 24-well microplates where twelve different conditions were tested. The reaction was allowed to take place for 2.5 h at room temperature in the absence of light. The UV-VIS spectra, mean size and zeta potential were determined for all conditions. **Table 2.2** specifies all the designed conditions in the microplate.

Table 2.2. Reaction parameters tested in the 24-well microplate assay.

Reaction	TE (%) (v/v)	[$AgNO_3$] (mM)	pH
1	0.25	1	8
2	0.25	1	9
3	0.5	5	11
4	0.5	10	11
5	4.55	1	11
6	4.55	5	11
7	5	1	9
8	5	10	9
9	5	1	11
10	5	1	12
11	12.5	5	11
12	4	8	11

2.2.3.1.3 Optimization of silver nanoparticles synthesis conditions

To optimize the synthesis and obtain AgNP with the intended characteristics, the impact of selected variables was evaluated separately, as one variable changed, and the others were kept constant (**Table 2.3**). All reactions occurred in 10 mL flasks under stirring. The formation of AgNP was confirmed by UV-Vis spectra, mean particle size and zeta potential.

Table 2.3. Reactions parameters for the variables tested.

Variable: Temperature: room or 37 ºC Fixed conditions: [TE]: 1.70% (v/v) [$AgNO_3$]: 1.67 mM Reaction time: 24h pH: 11	Variable: [$AgNO_3$]: 1-10 mM Fixed conditions: [TE]: 0.5% (v/v) Temperature: Room temperature Reaction time: 2h30 pH: 11
Variable: Reaction time: 15-180 min Fixed conditions: [TE]: 1.67% (v/v) Temperature: 65 ºC [$AgNO_3$]: 1.67 mM pH: 11	Variable: pH: 8 or 9 Fixed conditions: [TE]: 10% (v/v) Temperature: Room temperature [$AgNO_3$]: 5 mM Reaction time: 2h30

The final protocol for the biosynthesis of AgNP using TE produced by SWE is the result of all the data gathered in the above-described studies. The biosynthesis starts with the addition of 5 mL of TE, drop by drop, to a glass beaker with 245 mL of 1.6 mM of $AgNO_3$ (**Figure 2.1**). The pH was adjusted between 11.5 and 12, under magnetic stirring. Reaction time was set at 2.5 h in the absence of light at room temperature. At the end, the mixture was divided in 15 mL aliquots and moved to 250 mL Schott flasks. Then, these flasks are frozen at 80 ºC and freeze-dried during the night (Edwards Modulyo Freeze

Drier, Crawley, UK). In 15 mL of ultrapure-water, the mixture is suspended and centrifuged at 4000 rpm in a Super centrifuge (Beckman J2-MC, USA). The product is centrifuged three times. Pellets of each cycle of centrifugation are collected and kept at 4 ºC in the dark.

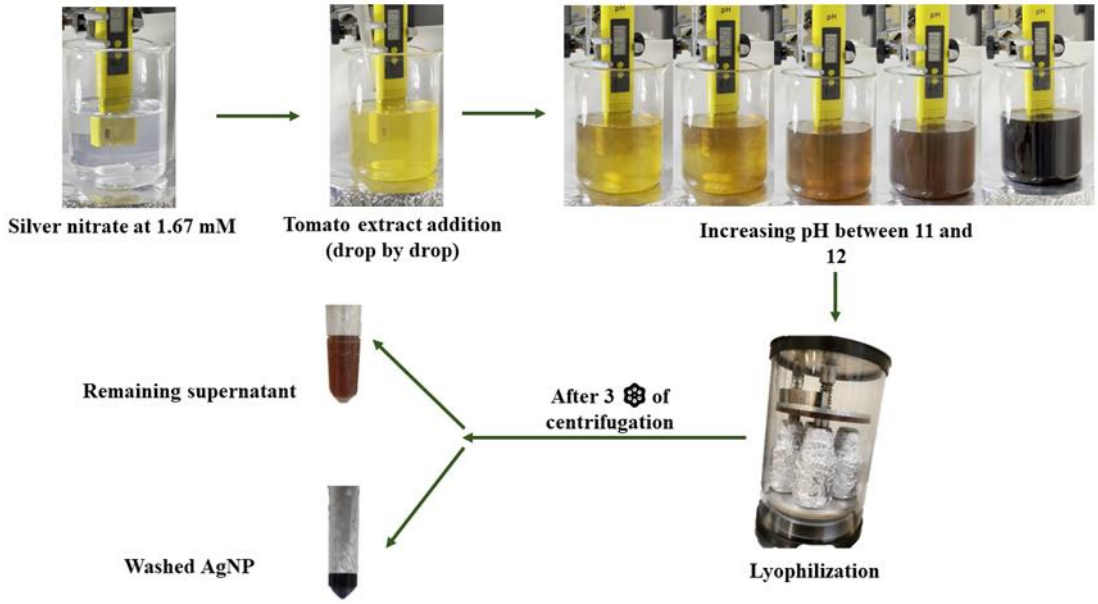

Figure 2.1. Schematic representation of AgNP biosynthesis and purification.

2.2.4 Silver nanoparticles characterization

2.2.4.1 UV-Vis spectrophotometry

In a quartz cuvette, AgNP were diluted in ultrapure water at 1:43 ratio. Wavelength of the absorption spectrum was set between 380-600 nm in the spectrophotometer (Shimadzu UV-160, Tokyo, Japan).

2.2.4.2 Mean size and zeta potential

Mean size and polydispersity index (PDI) values of AgNP were acquired in a Zetasizer NanoS (Malvern Instruments, Malvern, UK) equipment at 20 ºC. AgNP were diluted in ultrapure water at 1:50 ratio in a disposable cell. Both parameters were obtained by dynamic light scattering (DLS), at a detection angle of 173º to avoid scattered light signals from small particles, that introduces error in the amount of intensity detected. Using the Stokes-Einstein equation (**Equation 1**) and cumulants analysis, the hydrodynamic diameter (size of the particle) is acquired:

$$d(\mathrm{H}) = \frac{kT}{3\pi\eta D}$$

Equation 1. Stokes-Einstein equation.

Zeta potential of AgNP was acquired by laser-Doppler anemometry in Zetasizer NanoZ (Malvern Instruments®, UK). AgNP were diluted in ultrapure water at 1:50 ratio in a folded capillary zeta cell. Using Smoluchowski model (**Equation 2**), the software calculates this parameter:

$$U_E = \frac{2\varepsilon\zeta f(Ka)}{3\eta}$$

Equation 2. Smoluchowski model.

2.2.4.3 Quantification of AgNP

An aqueous suspension of AgNP was dried in an oven until it was transformed into a powder. A stock solution of 6 mg/mL AgNP solution was prepared to form a range of concentrations varying from 0.01 and 0.4 mg/mL. The absorbance was acquired at 450 nm with water being the blank [113].

2.2.4.4 Morphological analyses

The samples used for AFM were diluted in 1:10000 using ultrapure water. The mixture was poured into a glass treated with poly-L-lysine for 20 min. Afterwards, was rinsed with water and dried at room temperature. The quantification was executed in an Axiovert 200 inverted microscope (Carl Zeiss, Jena, Germany) containing NanoWizard II system (JPK Instruments, Berlin, Germany). The instrument is also supplied with a piezoelectric scanner with a linear z-range of 15 µm and an infrared laser. The measurements were implemented in intermittent tapping method. In this procedure, the surface of the sample is touched by the probe tip and the data generated is discrete. The material of the tip was silicon oxide with a 6 nm radius. The procedure was set with a resonant frequency of 60 kHz and constant energy of 3 Nm^{-1}. Data was evaluated with JPK v3 processor (JPK Instruments, Berlin, Germany).

The morphology of AgNP was also characterized by Transmission Electronic Microscopy (TEM). For TEM analyses, aliquots (10 µL) of AgNP suspensions were placed on Formvar/carbon coated grids and the excess solution was removed with a filter paper. Then, the material was negatively stained with 1% of uranyl acetate and left in room conditions for air-drying. Observations were carried out on a 1200EX transmission electron microscope (JEOL Ltd., Tokyo, Japan) operating at 80 kV and images were recorded digitally.

2.2.4.5 Chemical characterization of AgNP

AgNP were characterized in terms of total carbohydrates and phenolic contents as described in section **2.2.2**.

2.2.5 Biological activities of AgNP

2.2.5.1 *In vitro* cell viability of Human monocyte-like (THP-1) cell line

The cytotoxicity potential of the AgNP was evaluated in THP-1 cell line, a human acute monocytic leukemia cell line, obtained from ATCC (Barcelona, Spain). THP-1 cells were cultured in RPMI-1640 medium, supplemented with 10% inactivated fetal bovine serum (iFBS) and 1% penicillin-streptomycin (10,000 U/mL) and incubated at 37ºC in a humidified incubator with 5% CO_2 atmosphere. Cells were sub-cultured every week. In a 96-wells microplate, THP-1 were seeded at a concentration of $3x10^5$ cells/well and incubated for 48 hours in a RPMI medium with 50 ng/mL of PMA (phorbol 12-myristate 13-acetate) to promote differentiation into macrophages. After the 48 hours, the medium was removed, and the wells were washed with sterile PBS. Different concentrations of AgNP in PBS were tested (ranging from 181 to 2.83 µg/mL) and incubated again for 24 hours under the previous conditions. For the determination of viable cells, a MTT solution at 0.5 mg/mL was used. The addition of MTT produces formazan crystals, made by the cleavage of the tetrazolium ring of MTT. The reaction occurs in functioning mitochondria by dehydrogenases. The plates were incubated for 4 hours with 50 µL/well of the prepared MTT solution. The crystals were dissolved with 200 µL/well of DMSO and absorbances were measured at 570 nm in a Microplate Reader (BioTek® Instruments, USA).

2.2.5.2 *In vitro* cell viability in human keratinocyte (HaCaT) cell line

The cytotoxicity potential of AgNP was evaluated in HaCaT cell line, a non-tumorigenic adherent immortalized human keratinocytes cell line obtained from CLS (Eppelheim, Germany). The cells were cultured in Dulbecco's modified Eagle's medium (DMEM) plus GlutaMAX™ dipeptide (L-glutamine and L-alanine), rich in glucose, supplemented with 10 % iFBS and 1 % penicillin-streptomycin (10,000 U/mL) and incubated at 37ºC in a humidified incubator with 5% CO_2 atmosphere. Cells were seeded at a density of $3x10^4$ cells/well in a 96-well microplate and incubated until 60-70% of confluence was obtained. After the 24 hours, cells were exposed to the same concentrations of AgNP referred in section 2.2.5.1. Cells were incubated again for another period of 24 hours and then the wells were washed. The cell viability was assessed using the MTS assay kit (Promega®). MTS has the same principle as MTT. The difference is the formation of a soluble formazan that doesn't require DMSO and preserves the cells. A solution of MTS+PMS (20 µL) was added to each well and incubated at 37ºC for 2 hours. Absorbances were recorded at 490 and 630 nm in a Microplate Reader (BioTek® Instruments, USA).

2.2.5.3 *In vitro* anti-leishmanial activity against *Leishmania major* promastigotes

L. major amastigotes were obtained from lymph nodes of infected female BALB/c mice. Differentiation of amastigotes to promastigotes was performed at 26ºC in Schneider's medium supplemented with 1% penicillin-streptomycin, 2% sterile human urine, 10% iFBS. Promastigotes were sub-cultured weekly. AgNP were tested in *L. major* strain (MHOM/SA/85/JISH118). Parasites were seeded at a density of $2x10^6$/well in a 96-well microplate and incubated with the AgNP at concentrations ranging from 90.5 to 0.71 µg/mL for 72 hours. Afterwards, 20 µL/well of a 5 mg/mL MTT solution was added. After 4 hours, the plates were centrifuged at 2500 rpm, discarding most of the supernatant. To solubilize the formed crystals 200 µL/well of DMSO was added. Absorbances were measured at 570 nm in a Microplate Reader (BioTek® Instruments, USA).

2.2.6 MIC assessment by Broth Microdilution

The *in vitro* antimicrobial study was carried out using the Gram (+) bacteria *Staphylococcus aureus* (ATCC 25923) and the Gram (-) bacteria *Pseudomonas aeroginosa* (ATCC PAO1), both strains were obtained from ATCC (Barcelona, Spain). *S. aureus* was grown in Mueller Hinton broth (MHB) and *P. aeroginosa* in Lysogeny broth (LB) overnight at 37ºC. For each bacteria, a 96-well microplate was plated using a suspension of $5x10^5$ CFU/mL. Ten serial dilutions in 2-fold were performed using concentrations between 3.62 mg/mL and 0.0035 mg/mL. The plates were incubated at 37ºC for 18 hours. Controls were included in each plate: AgNP free (positive) and non-inoculated wells (negative). The minimum inhibitory concentration (MIC) defined as the lowest AgNP concentration that inhibited growth, was calculated for each strain.

2.2.7 Antimicrobial activity of AgNP assessed in an *ex vivo* model

To evaluate the antimicrobial activity the sterilizing action of AgNP was tested through an *ex vivo* porcine skin model [114]. The sterilization protocol was as described in **Figure 2.2**. MTT and histology were used to determine skin viability and irritation. Photographic images of skin were collected. AgNP (3.62 mg/mL) were compared to untreated skin soaked in PBS or in the TE used to produce AgNP, in ethanol (EtOH) 70% or 100%, and in 5% SDS. Two-step treatments were also explored. Skin specimens were superficially swabbed with a cotton swab and plated on tryptic soy agar (TSA).

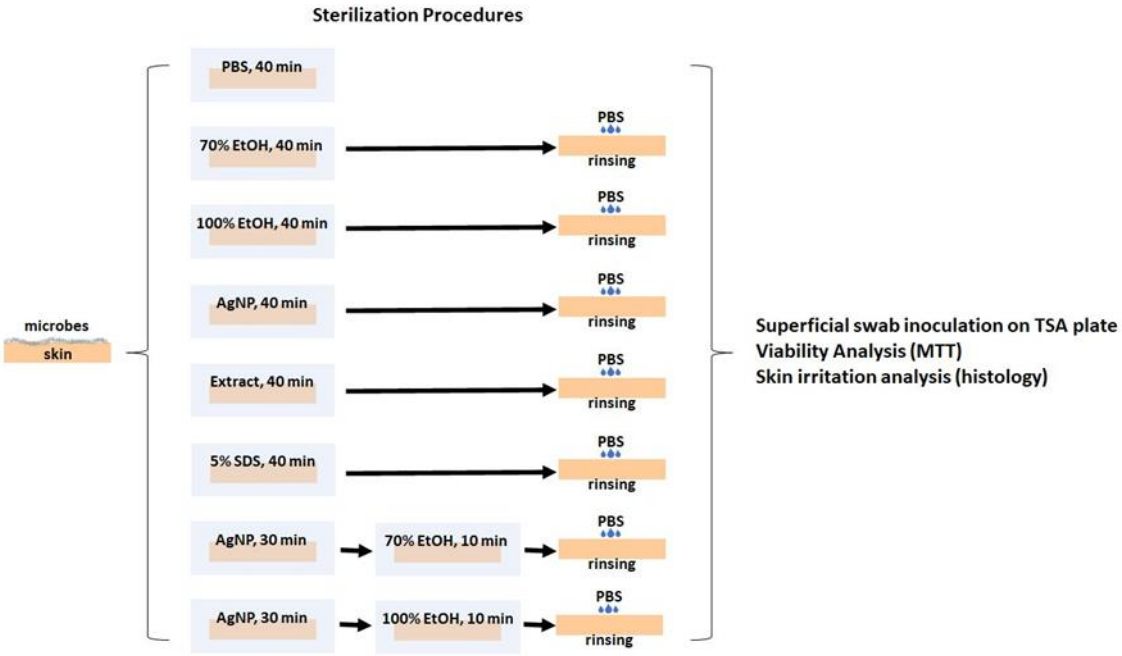

Figure 2.2.

Figure 2.2. Illustration of the procedure of *ex vivo* model.

Porcine skin was acquired from a supermarket. Eight portions of skin were cut, placed in petri dishes, and submerged in different solvents. PBS, 70% EtOH, 100% EtOH, AgNP, TE and 5% SDS were used to submerge different skin portions for 40 minutes. Two other skin portions were submerged in AgNP for 30 minutes. After that both were dried with a sterile gauze, and one was immersed in 70% EtOH and the other in 100% EtOH for 10 minutes (**Figure 2.2**). All skin specimens were washed with PBS and dried with a sterile gauze. The skin portions were incubated at 30ºC and the growth of microorganisms was evaluated for 14 days. Pictures of the skin were taken at days 0, 7, and 14, after sterilization procedure. Swabs of the skin surface were performed at days 0, 7 and 14, inoculated in TSA plates and incubated at 37 ºC. Pictures of the plates were taken at days 2, 9 and 17 for inoculations made on days 0, 7 and 14, respectively.

The skin viability and cutaneous irritation was assessed for histological analysis. In day 0, six biopsies were performed in each skin fraction after sterilization procedure. One biopsy of each group was stored in eppendorfs with 500 µL of formalin kept at 4ºC until the histological analysis. The remaining 5 biopsies were incubated in a 96 well microplate with 100 µL MTT at 37ºC for 3 hours. Then, 100 µL of HCl in 2-propanol was placed in the wells and incubated overnight at 4ºC. The skin was taken, and the plates were read at 570 nm.

2.2.8 Animal model of excisional wound

2.2.8.1 Preparation of AgNP gel

An aqueous AgNP suspension was mixed with Dermosoft™ (2%, w/w). Under vigorous stirring, Lecigel® (2% w/v) was added to obtain a hydrogel with 1.5 mg/mL of AgNP. The placebo was made with the described method, using water instead of AgNP. Characteristics of the hydrogel such as color and odor were tested. Using 713 pH meter from Metrohm (Filderstadt, Germany), the pH was analyzed at 20 °C.

2.2.8.2 Evaluation of therapeutic potential of developed nanoparticles using an *in vivo* wound healing model

Mice were anesthetized with isoflurane by inhalation. The dorsal skin was shaved and cleansed with PBS pH= 7.4 and a 1 cm line was made using a scalpel. The animals were randomly assigned in three different groups: the first group (n=3), the negative control, was administered with 100 µL of the placebo gel; the second group (n=3) was administered with 100 µL (1.5 mg/mL AgNP) of the AgNP gel; the third group (n=3), the positive group, was administered with 100 µL of Silvederma®, a commercial cream of silver sulfadiazine (10 mg/g). These administrations were made daily, from day (after incision) until day 6. Mice were accommodated individually with access to food and water *ad libitum*. Body weight was recorded from beginning until the end of the assay. During wounding and each following day, macroscopic wound photographs were taken (D4S model, Nikon, Tokyo, Japan) and the area measured (ImageJ software) to obtain chronological healing profile. At the end of the assay at day 7, mice were sacrificed. The wounded area was excised and handled for histological analysis. Hematoxylin & eosin staining was performed on 4 µm longitudinal tissue area. The assessment was accomplished by an independent pathologist.

2.2.9 Statistical analysis

For *in vitro* assays results were expressed as mean ± standard deviation (sd) of representative experiments. Statistical analysis was assessed by one-way ANOVA with all pairwise multiple comparison procedures. For *in vivo* experiments results were expressed as mean ± standard error of the mean (SEM). One-way ANOVA followed by Tukey's post-hoc test was used.

3

RESULTS AND DISCUSSION

3.1 Characterization of the tomato extracts

Total phenolic and carbohydrate compounds are important components of tomato extracts involved in the reduction and stabilization steps of the AgNP biosynthesis. To understand the impact of the subcritical water treatment in the extraction of these phytochemicals, a simple method without the use of temperature or pressure was used for comparison. This method consists in blending green tomatoes with an immersion blender producing a light green aqueous extract after centrifugation. The aqueous tomato extract prepared by subcritical water presents a deep brown color. The carbohydrate and phenolic content of both extracts were analyzed and compared. As reported in **Table 3.1**, the blended tomato extract contains more carbohydrates than the SWE tomato extract. One possible explanation is the chemical breakdown of the carbohydrates due to the elevated temperature and pressure during subcritical water process. On the other hand, results show that SWE TE has a much higher phenolic content than blended TE. This result suggests that the TE obtained by SWE is more concentrated in phytoconstituents and biomolecules relevant for the AgNP biosynthesis. The carbohydrates and phenolic content of both tomato extracts were determined using D(+)-Glucose and Gallic acid equivalents as standards to prepare the calibration curves respectively (**Appendix 1 and 2**).

Table 3.1. Carbohydrates content and phenolic content of SWE and blended tomato extract. Results are presented as mean ± sd of three independent experiments.

Sample	**Carbohydrates (mg GE/mL)**	**Phenolic (mg GAE/mL)**
SWE Tomato Extract	22.8 ± 2.9	2.1 ± 0.4
Blended Tomato Extract	33.2 ± 4.5	0.2 ± 0.0

GE: Glucose Equivalents; GAE: Gallic Acid Equivalents

Based on the previous information, the SWE TE was chosen to generate the AgNP. This extract is eight times richer in phenolic compounds than the blended TE, supporting a more efficient reduction of the silver ions into silver nanoparticles. Blended TE is only 1.5 richer in carbohydrates so the stability of

the silver nanoparticles is not expected to be highly affected by the loss of carbohydrates in the SWE process. The results suggest that SWE TE could produce more stable silver nanoparticles. Moreover, other biomolecules such as proteins, amino acids, alkaloids, enzymes, saponins, tannins, terpenoids and vitamins present in the SWE could also contribute to the formation and stabilization of the AgNP [115].

3.2 Biosynthesis of AgNP

In this study, the biosynthesis of AgNP using green tomato extract obtained by subcritical water treatment as reducing agent is reported. A solution of silver nitrate salt ($AgNO_3$) in deionized water was applied as the silver source (Ag).

3.2.1 Pre-formulation studies: 96-well microplate experiment

In a pre-formulation assay conducted using 96-well microplate, different concentrations of $AgNO_3$ and TE were tested originating AgNP with varied sizes and concentrations. Visually, it can be confirmed that pH 11 favored the reaction (**Figure 3.1**), as stronger brown color was developed and the characteristic surface plasmon resonance (SPR) absorbance peak presented higher intensity in the UV-Vis spectroscopy analysis [116]. All the wells presenting brown color and SPR bands with maximum absorbance at 430 nm indicated the presence of AgNP. The SPR peak of AgNP ranges from 300-600 nm and depends on the environmental conditions such as pH, size, shape, concentration of extract or silver nitrate [117]. The four samples that had SPR peak as shown in **Figure 3.1** were analyzed by DLS (**Table 3.2**).

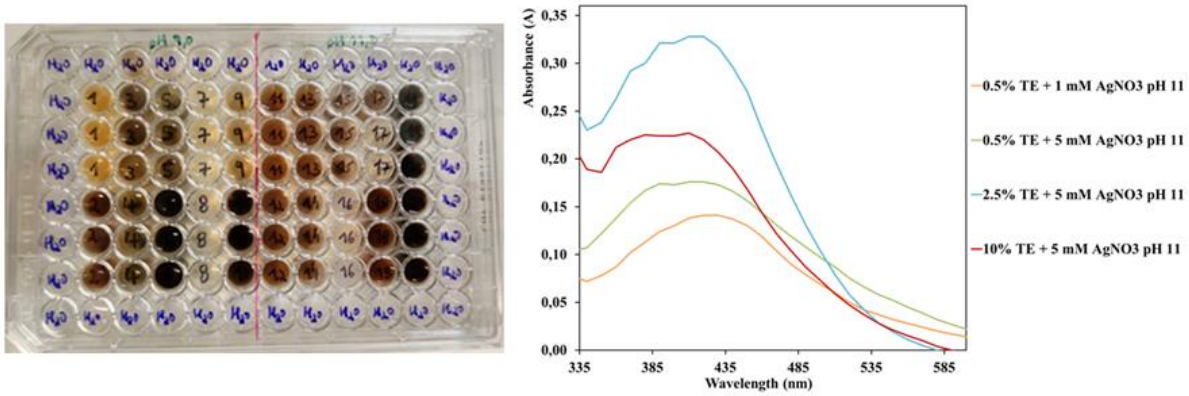

Figure 3.1. UV-Vis spectra and final color of the reactions tested in 96-well microplate. TE – tomato extract. In the micro-plate, reactions are numbered from the top to bottom, from left to right.

Reaction 18 led to the highest absorbance presented in **Figure 3.1** but the size of the AgNP was not above the desired value, as presented in **Table 3.2**. Possibly the higher size value is due to the presence of AgNP aggregates. Particles obtained from reactions 11 and 12 had ideal sizes although the

absorbance of the bands was lower. It has been shown that the AgNP dermal delivery performance relies on their physiochemical properties such as size and zeta potential and sizes between 20-80 nm proved to be effective [118,119]. In this study, the polydispersity index was high for all tested conditions, reveling some heterogenicity in size of the AgNP population. These preliminary results served as a refinement to a second pre-formulation assay tested in a 24-well microplate.

Table 3.2. Size and PdI of the AgNP for some reaction conditions tested in 96-well microplate.

Reaction	TE (%) (v/v)	[AgNO3] (mM)	Z-Average (nm)	PdI
11	0.5	1	23 ± 0	0.61 ± 0.01
12	0.5	5	29 ± 6	0.5 ±0.19
18	2.5	5	1010 ± 636	0.76 ± 0.17
19	10	5	-	-

3.2.2 Pre-formulation studies: 24-well microplate experiment

For 24-well microplate pre-formulation assay, twelve different syntheses were tested. Size, zeta potential and UV-Vis spectra were used to assess formation and stability of AgNP. The UV-Vis spectra of the conditions with SPR identification peak are depicted in **Figure 3.2**.

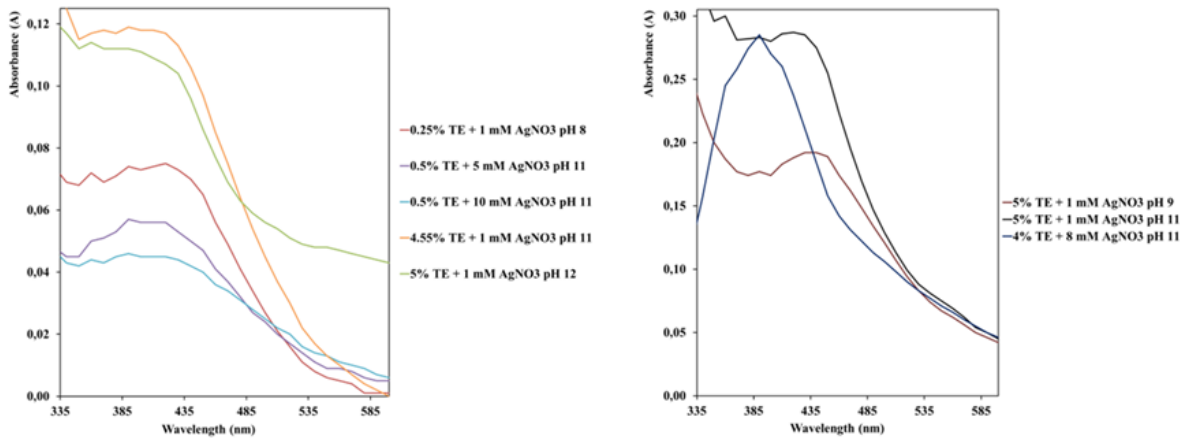

Figure 3.2. UV-Vis spectra of the reactions tested in 24-well microplate.

It is generally recognized that nanoparticle having mean sizes between 50 and 150 nm pass the various skin layers and reach the phagolysosomes of macrophages [120]. Zeta potential values above -30 mV are advantageous for the stabilization of nanoparticles and to prevent aggregation [121]. A PdI lower than 0.5 refers to a nanoparticle population not very dispersed in size and does not affect its efficacy when applied to the skin [122]. All reactions reported in **Table 3.3** presented both sizes and PdI within the required values for skin application. However, only reactions 6, 8 and 9 fulfilled all abovementioned characteristics of stable nanoparticles.

Table 3.3. Size and PdI of the reactions tested in 24-well microplate.

Reaction	pH	TE (%) (v/v)	[AgNO3] (mM)	Z-Average (nm)	PdI	ZP (mV)
3	11	0.5	5	96 ± 8	0.37 ± 0.06	-0.3 ± 0.5
4	11	0.5	10	69 ± 2	0.46 ± 0.01	-0.6 ± 0.2
5	11	4.55	1	143 ± 1	0.40 ± 0	-10.3 ± 0.6
6	11	4.55	5	49 ± 0	0.48 ± 0	-28.5 ± 1.8
8	9	5	10	111 ± 1	0.24 ± 0	-36.8 ± 0.1
9	11	5	1	160 ± 3	0.32 ± 0.03	-30.9 ± 0.3

The reactions not listed in **Table 3.3** and their characteristics can be found in **Appendix 3**.

3.3 Study of the impact of different parameters in the biosynthesis of AgNP

It has been already demonstrated that by varying key conditions/parameters in the biosynthesis of AgNP it is possible to change dramatically the characteristics of the particles obtained [123]. In the pre-formulation assays, it was possible to establish an optimal value for TE and with such fixed concentration different experimental conditions were tested, namely the effect of the temperature, pH, time of reaction and concentration of $AgNO_3$. This allowed the selection of the best conditions for the biosynthesis of silver nanoparticles using this TE.

The effect of the temperature, using 1.70% (v/v) TE and 1.67 mM $AgNO_3$, on the SPR peak is presented in **Figure 3.3-A**. The reaction was carried out for 24 h, in the dark, at pH 11. The size and PdI of AgNP (**Table 3.4**) produced at 37ºC were smaller than the AgNP produced at room temperature. The zeta potential of AgNP produced at both temperatures were negative (< -20 mV), indicating that they can be considered stable. The intensity of the SPR peak is higher at 37ºC which is in accordance with what has been found in other studies that correlate elevated temperatures with increased production rate of monodisperse and smaller-size nanoparticles [124].

In **Figure 3.3-B**, the SPR peaks resulting from different concentrations of silver nitrate tested in reaction mixtures with 0.5% (v/v) of TE, at room temperature are presented. The reaction time was 2h30, in the dark at pH 11. The SPR peak observed for the 1 mM concentration is narrower. The size difference of AgNP produced with 1 mM and 5 mM is minimal (**Table 3.4**). When the $AgNO_3$ concentration is higher (10 mM), a reduction in the SPR peak may indicate the depletion of the biomolecules in the TE that cannot maintain the AgNP formation [125].

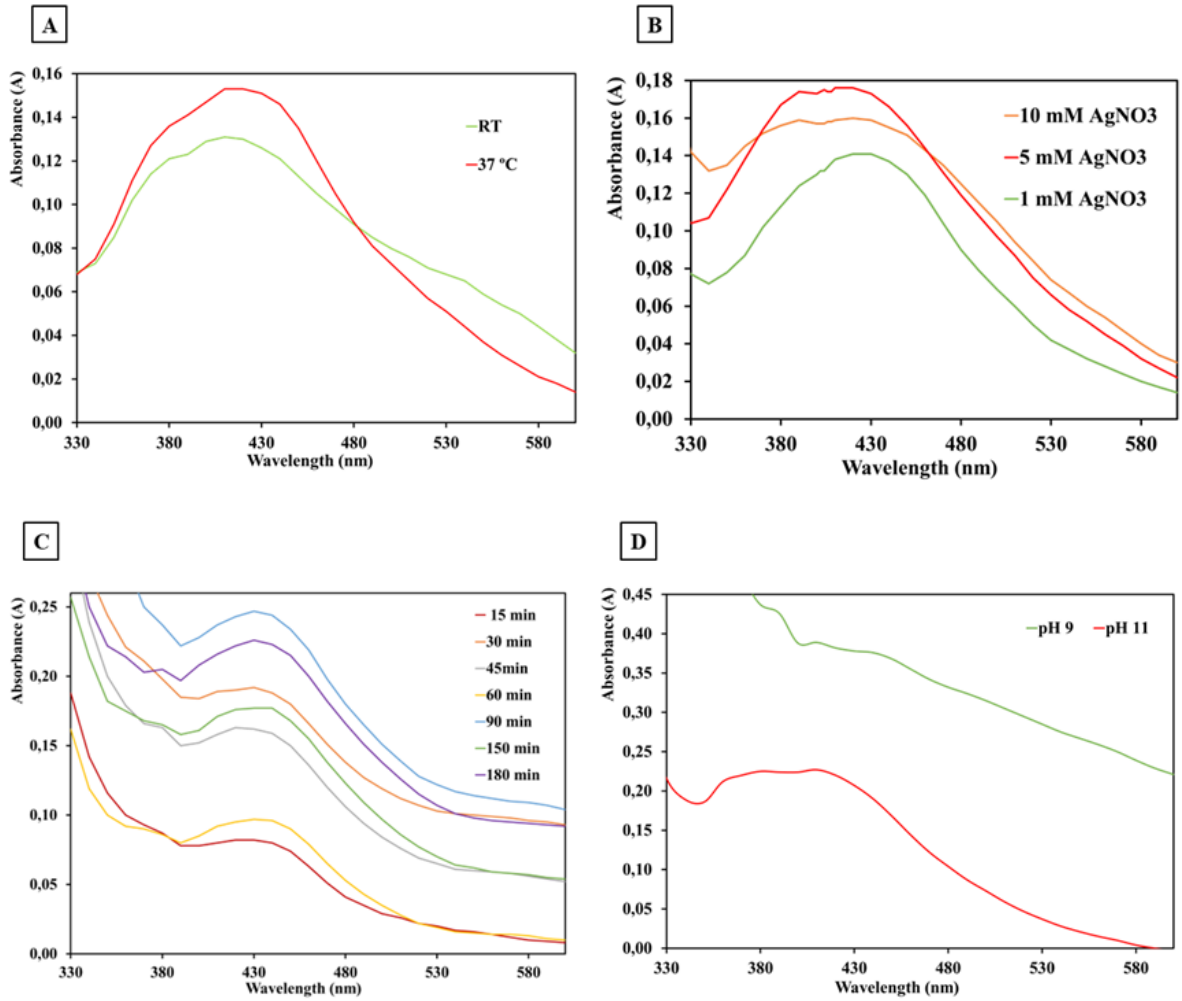

Figure 3.3. UV-Vis spectra, of AgNP produced under different reaction conditions. **(A)** Effect of Temperature; **(B)** Concentration of AgNO3; **(C)** Reaction time; **(D)** pH.

Table 3.4. Reaction parameters, mean size, PdI and zeta potential of AgNP obtained from TE and $AgNO_3$.

Manipulated Parameter		Z-Average (nm)	PdI	Zeta Potential (mV)
Time	15 min	163 ± 22	0.32 ± 0.08	-22 ± 1
	30 min	235 ± 47	0.29 ± 0.04	-28 ± 1
	45 min	272 ± 82	0.33 ± 0.02	-29 ±1
	60 min	222 ± 25	0.30 ± 0.03	-28 ± 1
	90 min	191 ± 27	0.29 ± 0.02	-29 ± 1
	120 min	290 ± 35	0.36 ± 0.07	-29 ± 3
	150 min	246 ± 34	0.34 ± 0.04	-32 ± 0
Temperature	Room	51 ± 1	0.34 ± 0.05	-29 ± 1
	37 ºC	35 ± 0	0.31 ± 0.03	-21 ± 3
$AgNO_3$	1 mM	23 ± 1	0.61 ± 0.01	-
	5 mM	29 ± 6	0.50 ± 0.19	-
	10 mM	-	-	-

The effect of reaction time was evaluated using 1.67% (v/v) of TE and 1.67 mM $AgNO_3$ at 65 ºC in the absence of light (**Figure 3.3-C**). The pH of the solution was 11. One of the observations taken from

results in **Table 3.4** is that the zeta potential increases with reaction time and PdI is almost constant. Temperature increases the rate of the reaction, but time is also crucial to develop stable AgNP [126]. Different pH values were evaluated using 10% (v/v) of TE poured into 5 mM $AgNO_3$ as shown in **Figure 3.3-D**. The reaction time was 150 minutes in the absence of light, at room temperature. The presence of the SPR peak is only visible when the reaction was performed at pH 11. With the results of the previous experiments, it was determined that the biosynthesis of silver nanoparticles is favored with alkaline pH, in accordance to previously published data [127].

As a result of the above reported optimization studies, the AgNP for further characterization were biosynthesized using 5 mL of TE, corresponding to 2% (v/v), 245 mL of 2 mM $AgNO_3$ solution, at room temperature, for 150 minutes, at pH 11, under constant stirring.

3.4 Physiochemical characterization of optimized AgNP

The AgNP formation was monitored by measuring the SPR in the UV-Vis region and characterized in terms of size distribution by DLS, shape and state of aggregation, through atomic force microscopy (AFM) and transmission electron microscopy (TEM) analysis, respectively. The stability of AgNP solutions was also evaluated through zeta potential analysis.

3.4.1 UV–Vis analysis

As shown in **Figure 3.4** the biosynthesized AgNP have a SPR peak located between 402-406 nm. This wavelength range suggests that the average size of AgNP produced is homogeneous since the peak is narrow. The SPR peak of small nanoparticles appears in lower wavelengths and vice-versa [128]. The nanoparticles shape is influenced by the size and agglomeration. Some AgNP produced have a larger size, scattering more light, producing a broader SPR peak [129].

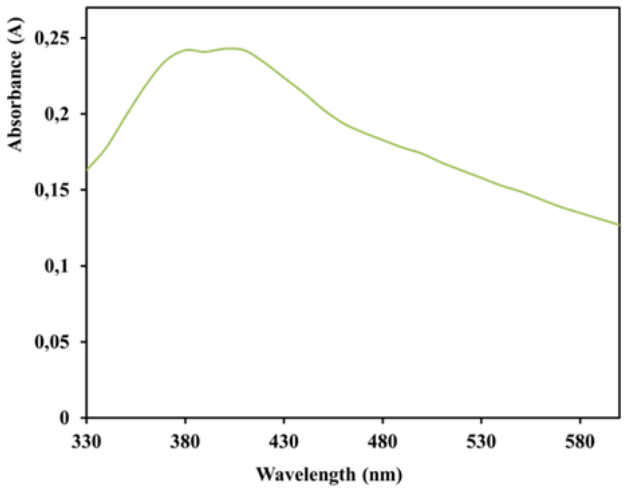

Figure 3.4. UV−vis absorption spectrum of biosynthesized AgNP using TE and $AgNO_3$ at room temperature after 150 minutes at pH 11.

A calibration curve (**Figure 3.5**) using different concentrations of dried AgNP was made to determine the concentration of the AgNP suspension. Using the equation obtained from linear regression, the concentration of prepared AgNP was determined to be 3.62 mg/mL.

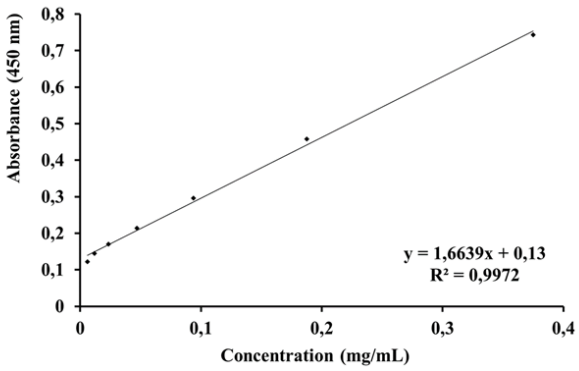

Figure 3.5. Calibration curve for AgNP quantification.

3.4.2 Carbohydrates and phenolic content of AgNP

The carbohydrates and phenolic content of AgNP presented in **Table 3.5** are lower compared to the values obtained for the TE used in their synthesis (presented in **Table 3.1**). However, the presence of these biomolecules in the AgNP suspension indicates they contribute to the biosynthesis as reduction and stabilization agents of the nanoparticles [130–132].

Table 3.5. Carbohydrates content and phenolic content of the AgNP. Results are presented as mean ± sd of three independent experiments.

Sample	Carbohydrates (mg GE/mL)	Phenolic (mg GAE/mL)
AgNP	0.07 ± 0.04	0.2 ± 0.2

GE: Glucose Equivalents; GAE: Gallic Acid Equivalents

3.4.3 Particle size and zeta potential characterization

Table 3.6 presents results regarding particle size, PdI and zeta potential of AgNP. DLS was used to determine the mean particle size and PdI of the AgNP solution, which was found to be 60 nm, and 0.522 respectively (**Figure 3.6**). This technique is a simple and fast method used to determine nanoparticles size. It can also be used to determine the thickness of the capping or stabilizing layer surrounding metallic particles [133].

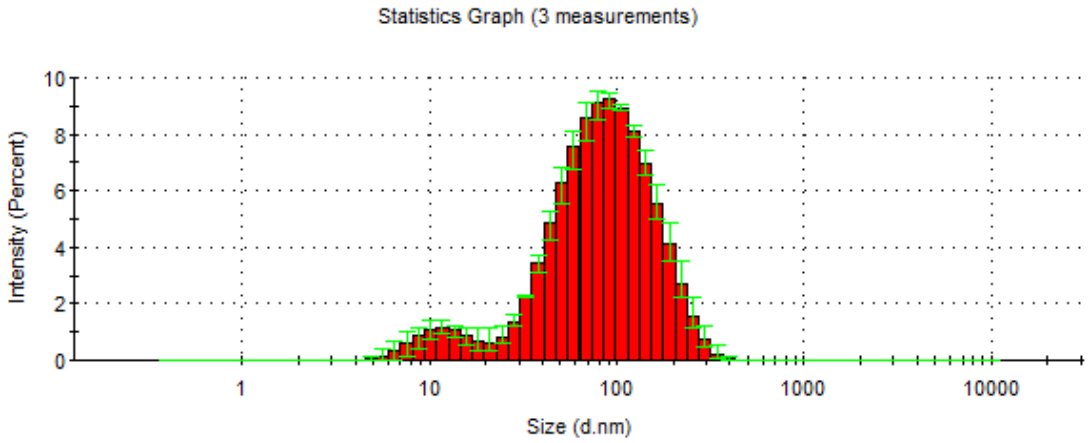

Figure 3.6. Particle size distribution histogram

The small size of theses nanoparticles is ideal to penetrate the skin. The PdI is around 0.5, which is reasonable within the criteria defined and indicates their relatively uniform dimensions. The zeta potential value is a measure of the surface charge of the synthesized AgNP, which promotes the stability in the suspension. The negative zeta potential exhibited provides repulsive electrostatic stabilization for the AgNP (**Table 3.6**).

Table 3.6. Particle size, PdI and zeta potential of AgNP.

Z-Average (nm)	PdI	Zeta Potential (mV)
60 ± 17	0.522± 0.052	-42 ± 4

3.4.4 Morphological analysis

Atomic force microscopy (AFM) and transmission electron microscopy (TEM) were used to characterize the shape, size, and distribution of the AgNP. In **Figure 3.7**, AFM and TEM micrographs confirm that the nanoparticles have a round shape. In TEM, the estimated nanoparticle size is 80 nm while in AFM, the median size is 83 nm. In the literature, difference size between DLS and TEM/AFM is common and could be derived from non-homogeneous dispersion of the samples [134].

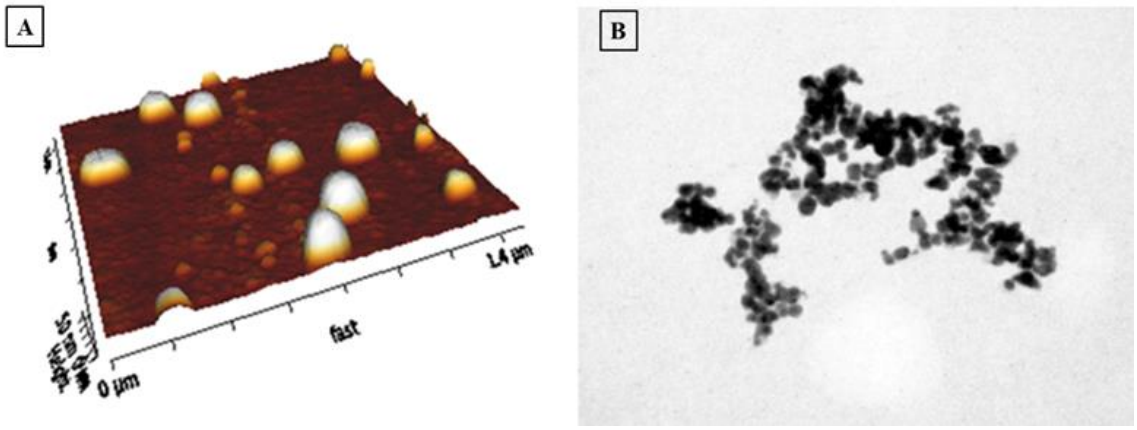

Figure 3.7. Physiochemical characteristics of biosynthesized silver nanoparticles: **(A)** Image of AgNP diluted 1/10000 obtained by atomic force microscopy (AFM); **(B)** Micrographs of AgNP acquired by transmission electron microscopy (TEM).

3.5 *In vitro* biocompatibility assays

The cytotoxicity of AgNP was first investigated *in vitro* against two human cell lines. A keratinocyte cell line (HaCaT) and was used since the biosynthesized AgNP are intended for topical application, thus it is critical that they are safe for skin cells. The human leukemia monocyte cell line THP-1 was used as host cell for *Leishmania* parasite as is considered a valid model for *in vitro* drug screening against leishmaniasis [135]. In a second round of experiments and after determining the CC_{50} values for both human cell line, the anti-parasitic effect of the AgNP was determined *in vitro* against *L. major* promastigotes in culture.

These assays were performed using the MTT colorimetric assay for THP-1 cells and *L. major* parasites. In the case of HaCaT cells, the MTS colorimetric assay was used due to technical incompatibilities.

The cellular viability results for HaCaT and THP-1 macrophage-like cells exposed to AgNP are shown in **Figure 3.8**. AgNP did not show toxic effects in the range of investigated concentrations in HaCaT cells. For THP-1 cells, results in **Figure 3.8** show a reduction in cell viability in a dose-dependent manner with around 100% viability at the lower concentration down to around 50% at the highest AgNP concentration tested. Overall, these findings indicate that the AgNP are not cytotoxic for the macrophages and for the skin cells.

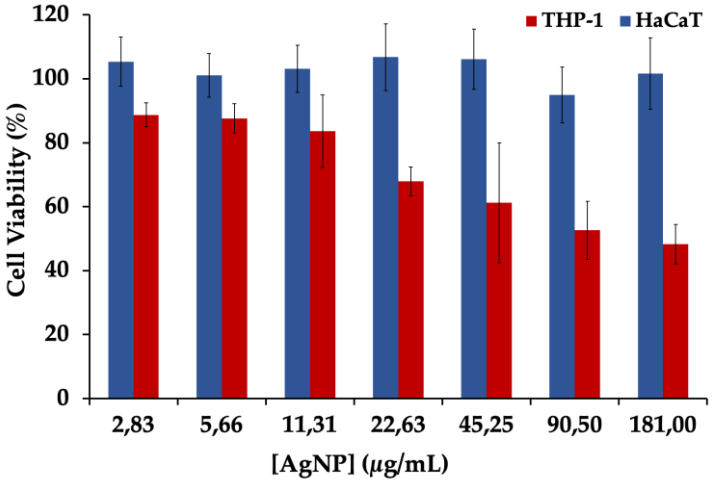

Figure 3.8. Evaluation of AgNP cytotoxicity in mammalian cell lines. The effect of increasing concentrations of AgNP on the viability of HaCaT (blue columns) and THP-1 (red columns) cells exposed for 48 hours. Percent cell viability was calculated relative to the control using a colorimetric assay. Data is expressed as the mean ± sd of 3 independent measurements.

As displayed in **Figure 3.9**, the AgNP were active against *L. major* promastigotes reducing parasite viability to around 40% with a concentration of 45.25 µg/mL. This is a good indicator that the AgNP are more toxic to the parasites than to mammalian cells [136–138].

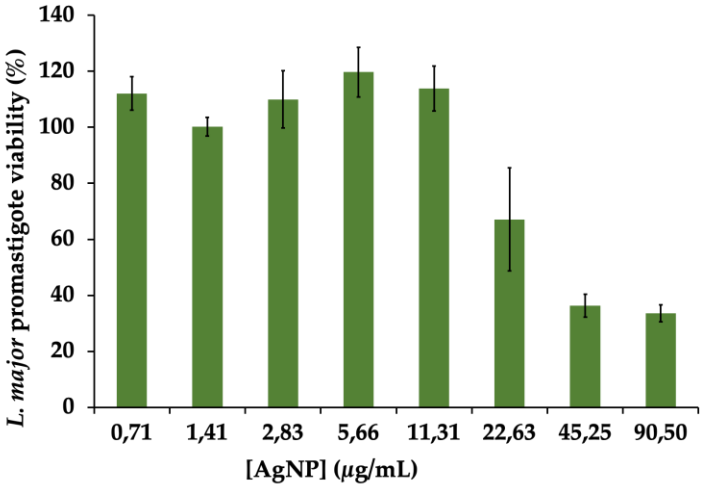

Figure 3.9. Anti-leishmanial effect of AgNP against *L. major* promastigotes after 72 hours of incubation. Percent cell viability was calculated relative to the control using the MTT assay. Data is expressed as the mean ± sd of 3 independent measurements.

Table 3.7 summarizes the cytotoxicity effects of AgNP in human cells and the activity against *Leishmania* parasites.

Table 3.7. In vitro CC_{50} values for THP-1 and HaCaT cells, and IC_{50} values for *L. major* promastigotes of AgNP

Sample	HaCaT CC_{50} (µg/mL)	THP-1 CC_{50} (µg/mL)	*L. major* promastigotes IC_{50} (µg/mL)
AgNP	> 181	146.03	33.22

CC_{50}: 50% cytotoxic concentration; IC_{50}: 50% inhibitory concentration

These results show that AgNP are more toxic for *Leishmania* parasites than for mammalian cells indicating that is possible to treat CL skin lesions with no damage to skin cells.

3.6 *In vitro* antimicrobial activity

The susceptibility of *S. aureus* and *P. aeroginosa* results are reported in **Figure 3.10**. The AgNP did not inhibited the growth of *S. aureus* in the tested concentrations. However, the MIC was possible to be determined when *P. aeroginosa*, was exposed to 0.0141 mg/mL AgNP. These results are in accordance with reports found in the literature [139–141] where AgNP are described to be more efficient in Gram(-) bacteria than Gram(+). This can be justified by differences in the wall thickness of bacteria. The Gram(+) bacteria wall is almost 8 times thicker than that of Gram (-) [142]. These results are quite promising considering possible treatments of skin infections caused by Gram(-) bacteria.

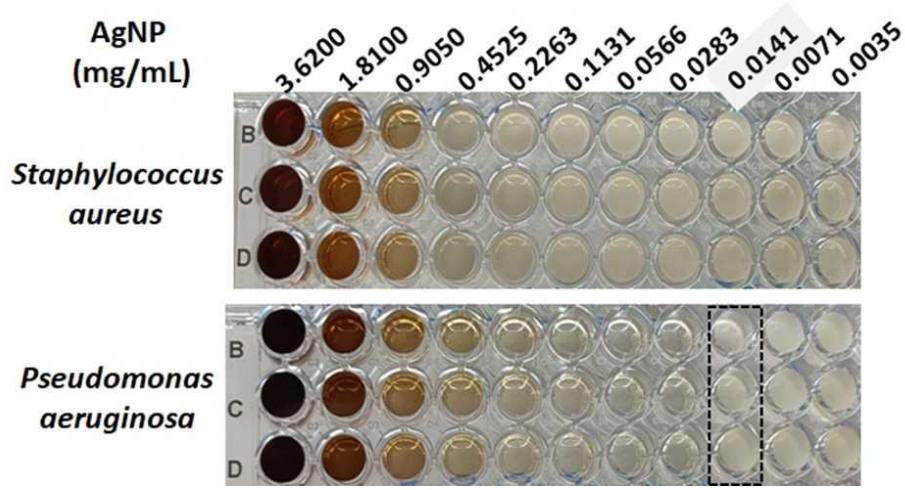

Figure 3.10. Microscopic appearance of bacterial growth in the presence of AgNP, measured on broth microdilution assay. From left to right, the concentration of AgNP decreases.

3.7 Antimicrobial activity of AgNP evaluated in an *ex vivo* skin model

AgNP have been proposed as an excellent antimicrobial agent against bacteria *in vitro* and *in vivo* and scientific achievements have been plenty revised [143]. However, the consequences of AgNP in the skin and their penetration have only been studied *in vitro*, mainly using skin cell lines. In this work, the antimicrobial effect of developed AgNP after topical application was compared to other solutions used in disinfection of tissues and surfaces and with skin irritant solutions, in an *ex vivo* model using full thickness pig skin [144] initially developed to study skin bacterial translocation. PBS was used as a control. The schematic representation of the procedure is presented in **Figure 2.2** in methods section. **Figure 3.11** shows the aspect of the skin incubated at 30 ºC for 14 days and from which at defined time points, a swab was cultured in TSA plates.

Figure 3.11. Images of the skin portions at day 0, day 7 and day 14 after the procedure.

Images from day 0 (**Figure 3.11**) were taken just after the soaking procedures and as can be observed, black staining is present in skin specimens treated with AgNP solution, more pronouncedly on sample just treated with AgNP. At day 7, the skin treated with extract already had colonies that could be seen at the naked eye. This rapid microorganism growth is explained by the high concentration of TE phytochemicals. All skin samples were darker, but ethanol treated samples present a more preserved aspect. Through the days, the skin decay is more apparent. The skin portions submerged in 70% EtOH and 100% EtOH had less decay. The skin portion submerged in AgNP looks similar to the result of 5% SDS. The skin portion submerged in extract, AgNP + 70% EtOH and AgNP + 100% EtOH looks similar to the control skin.

Chemical disinfectants can alter the skin structure and skin cell viability. Using an MTT assay, the viability of the cells (**Figure 3.12**) was evaluated to understand which condition had the least impact on the skin cells. Although the skin fractions that had EtOH looked more preserved, the skin viability is much inferior. The viability of the skin cells is almost 80% with 100% EtOH and 5% SDS. The lower viability of the study (<60%) was obtained with AgNP + 70% EtOH. In contrast, AgNP and extract have a skin viability similar to PBS, almost 100%. This result shows that AgNP (non-diluted) do not compromise the skin cells viability as measured in an *ex vivo* model.

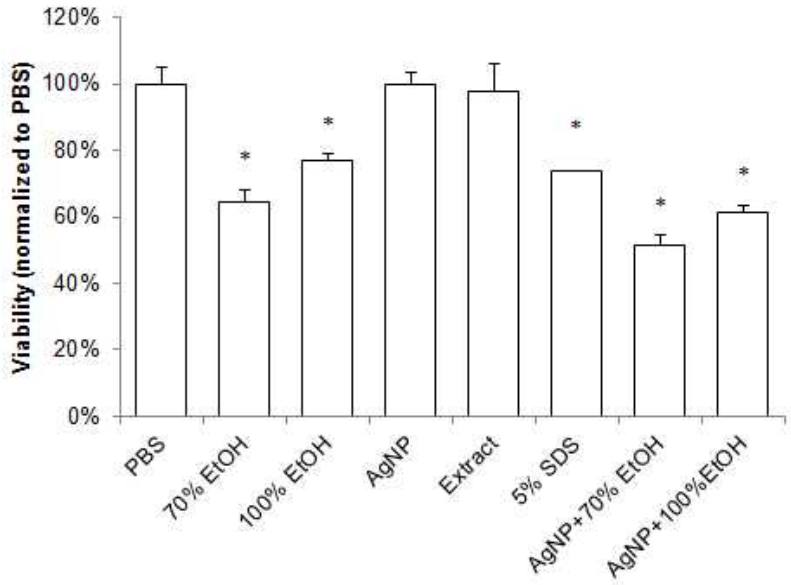

Figure 3.12. Analysis of skin tissue viability after sterilization procedure, compared with no-treatment control (PBS). Viability analysis is plotted as mean ± sd. Statistical analysis: * $p < 0.001$ vs PBS.

The swab tests (**Figure 3.13**) had the purpose of assessing the sterilization that each solution provided during the time course of the assay. At day 0 skins treated with 70% EtOH, 100% EtOH, AgNP + 70% EtOH and AgNP + 100% EtOH solutions show no growth of microorganisms. The skin portions treated with TE or 5% SDS presented comparable results, showing some microbial growth. PBS and AgNP presented comparable results, showing more colonies than the previous solutions. At days 7 and 14, plates from PBS, TE, 5% SDS and AgNP present similar aspect, and the microbial growth is equivalent.

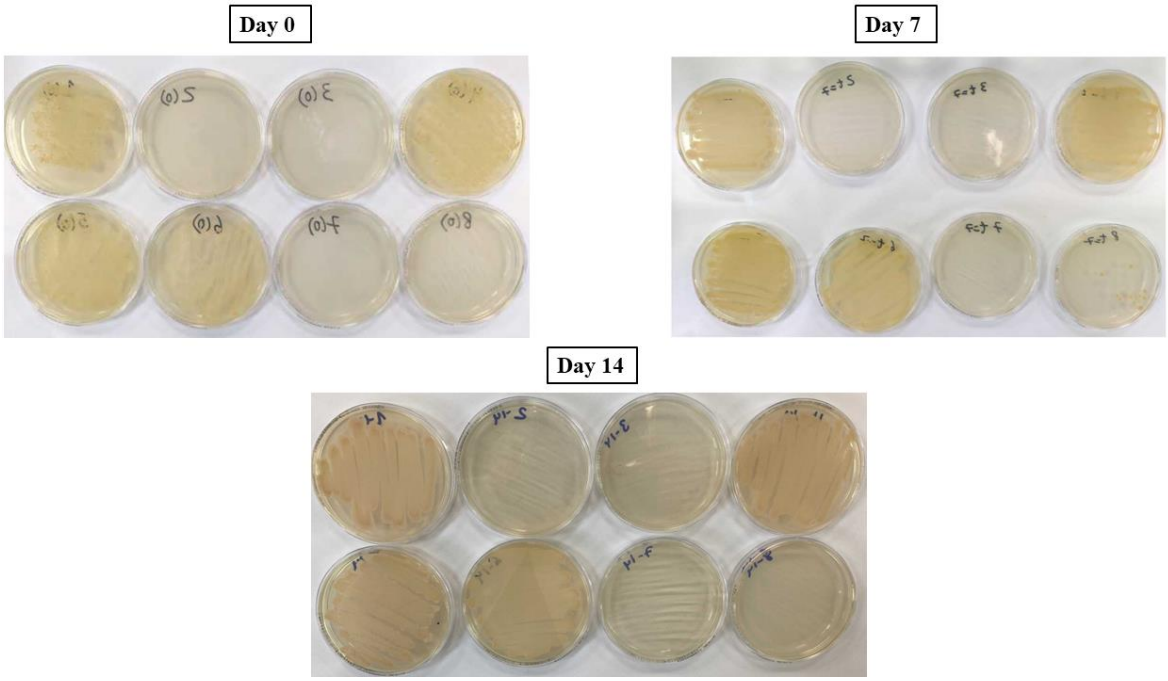

Figure 3.13. Microbial growth on TSA agar from swabs of the skin pork portions, where, in each image (top row, from left to right) **1-** PBS for 40 minutes immersion; **2-** 70% EtOH for 40 minutes immersion; **3-** 100% EtOH for 40 minutes immersion; **4-** AgNP for 40 minutes immersion; (bottom row, from left to right) **5**- Extract for 40 minutes immersion; **6**- 5% SDS for 40 minutes immersion; **7**- AgNP for 30 minutes + 70% EtOH for 10 minutes immersion; and 8- AgNP for 30 minutes + 100% EtOH for 10 minutes immersion.

The histological results were crucial to determine the cutaneous irritation of the solvents used (**Figure 3.14**). It is recognized that the source of porcine skin can have a substantial impact both on contamination, epidermis structure and usable time. Compared to PBS (**Figure 3.14-A**), 70% EtOH, 100% EtOH, AgNP and 5% SDS, the superficial layer contracted. The extract, AgNP + 70% EtOH and AgNP + 100% EtOH and extract didn't have alterations in the thickness of the layers, when compared to PBS. These results show that AgNP with EtOH can decrease the EtOH cutaneous irritation potential.

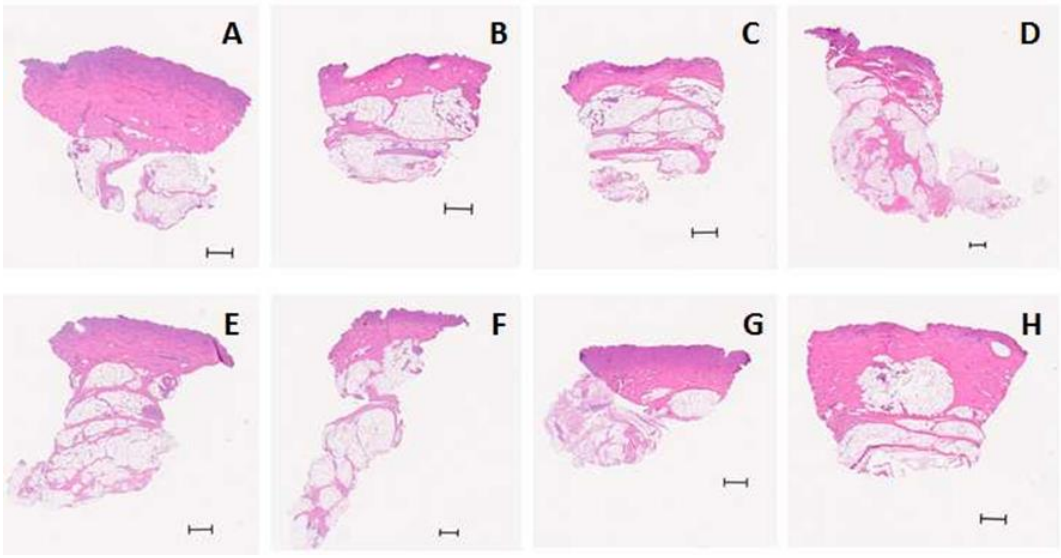

Figure 3.14. H&E stained microphotographs (in each picture the bar corresponds to 500 µm) from skin treated with different conditions: **A**- PBS for 40 minutes immersion; **B**- 70% EtOH for 40 minutes immersion; **C**- 100% EtOH for 40 minutes immersion; **D** - AgNP for 40 minutes immersion; ; **E**- Extract for 40 minutes immersion; **F**- 5% SDS for 40 minutes immersion; **G**- AgNP for 30 minutes + 70% EtOH for 10 minutes immersion; and **H**- AgNP for 30 minutes + 100% EtOH for 10 minutes immersion.

3.8 Wound healing effect of AgNP in a murine incisional acute wound model

Wound healing preclinical *in vivo* research commonly uses mice models either incisional or excisional [145]. In order to formulate AgNP in a semisolid pharmaceutical form, a hydrogel containing AgNP and the respective placebo were prepared. The macroscopic appearance of the gels is presented in **Figure 3.15**.

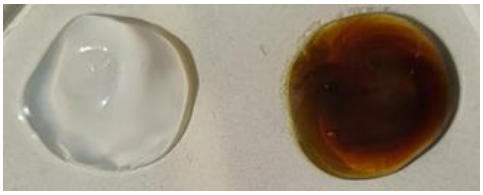

Figure 3.15. Macroscopic appearance of the gels used in the wound healing *in vivo* assay. The gel on the left is placebo and the gel on the right contains AgNP.

Semisolid formulations are convenient forms for topical applications since increase the drug residence time on the skin [146]. The gel composition was selected from a previous study as it shown compatibility with human skin without any irritation signs [147]. A gel containing 1.5 mg/mL AgNP was used to assess the healing performance of AgNP. The topical administration started in day 0 and wounds were treated in the following 7 days. **Figure 3.16 left panel** shows representative photos of the incision for the distinct groups at different time points. During the assay, the body weight variation was smaller than 10% and not statistically different between the groups (data not shown). As can be depicted from the **Figure 3.16, Graphic**, mice treated with placebo had a higher wound area, quite different from mice

treated with Silvederma® or AgNP ($p<0.05$). Statistically, there's no difference between Silvederma® and AgNP. Non-treated wound increases the area in the initial 2-3 days, indicator of variable expansion of wound margins [145]. This phenomenon was not observed in the groups treated with Silvederma® or AgNP. The placebo wounds did not complete closure during the time of the trial. Silvederma® has more silver incorporated than AgNP gel and both ensured rapid wound closure. These results are very encouraging and highlight the potential of AgNP in wound healing.

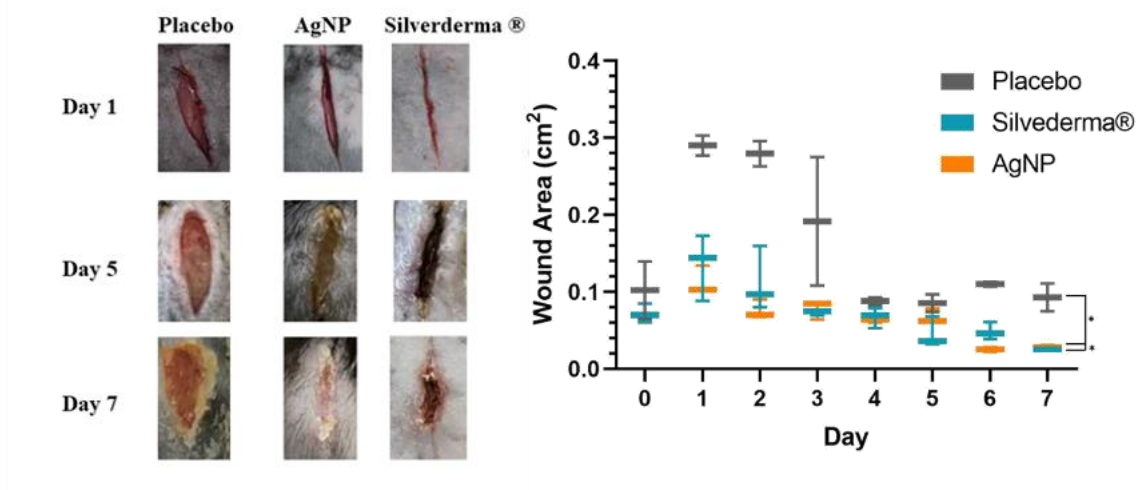

Figure 3.16. Left panel: Representative images of the incisional wound at days 1, 5 and 7 of the placebo (vehicle of AgNP gel), AgNP gel and Silvederma® cream (silver sulfadiazine 10 mg/g). **Graphic:** Wound area from placebo gel, Silvederma® cream and AgNP gel treated mice. Data is expressed as the mean ± SEM of 3 independent measurements. Statistics: one-way ANOVA followed by Tukey's post-hoc test. *$p < 0.05$ vs control

The histological results confirm that wound closure was successful in the groups treated with AgNP and Silvederma®. **Figure 3.17-A** shows that the wound treated with placebo did not close. The healing process looks more advanced with the AgNP formulation compared with sulfadiazine. The histological analysis corroborates results obtained in the wound area evaluation (**Figure 3.16**).

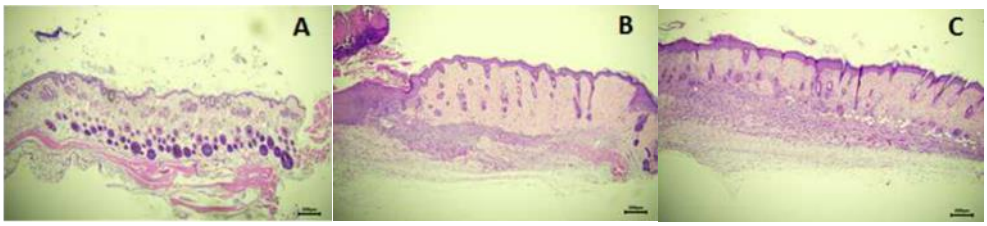

Figure 3.17. Images of histological sections of incisional wounds, after 7 days of administration: **(A)** placebo gel; **(B)** Silvederma® cream (silver sulfadiazine 10 mg/g); **(C)** AgNP formulation.

4

CONCLUSION

The demand for sustainable production of therapeutics is increasing. The biosynthesis of nanoparticles is an opportunity to use upcycling of industry waste since plants are rich in terpenoids, alkaloids and phenolics and any part can be used for the synthesis. This type of synthesis can also overcome the toxicity associated to chemical synthesis. The biogenic silver nanoparticles have interesting pharmacological features that look promising for topical treatment of skin diseases.

The unique chemical composition of plant-extract affects the characteristics and properties of the AgNP. To the best of our knowledge this is the first report on the use of a green tomato-derived extract obtained by subcritical water treatment for the biosynthesis of metallic nanoparticles. This subcritical water extraction process preserved the phenolic content of green tomato extract. The pre-formulation studies elucidated the role of the main parameters involved in the biosynthesis of AgNP, namely pH, silver nitrate concentration, time, and temperature. The AgNP formation can be confirmed by color change and an SPR peak. The AgNP produced had a proper size, a reasonable polydispersity index and good stability, confirmed by the value of zeta potential. AFM and TEM confirmed that AgNP had a round shape and the size distribution was homogeneous. The size obtained by this method can be considered suitable for topical administration. *In vitro* assays confirmed that AgNP are safe to human cells. Moreover, the IC_{50} obtained for *L. major* promastigotes, suggests AgNP anti-parasitic properties. *In vitro* antimicrobial activity showed susceptibility of Gram(-) bacteria to biogenic AgNP. The *ex vivo* antimicrobial assay reinforces the safety of AgNP after topical application. The *in vivo* assay demonstrated good wound-healing properties, comparable to commercial silver base topical formulations. In this study, it was demonstrated the potential of an industrial waste (green tomato) to be used in a green approach to the biosynthesis of AgNP under simple and eco-friendly conditions. The developed AgNP revealed antimicrobial, anti-parasitic and wound healing properties with an adequate profile for topical application. All these features are part of the requirements for a candidate treatment for cutaneous leishmaniasis, making these AgNP a valuable strategy in this research area.

5

FUTURE WORK

The present study opened new perspectives on the biosynthesis of AgNP using an unexplored biomass to extract phytocompounds, crucial as reducing and stabilizing agents. A complete characterization of green tomato extract is then essential to further optimize the conditions of AgNP synthesis. Antimicrobial activity of developed nanoparticles was assessed but further studies are needed to identify other susceptible species. It is also important to perform an *in vitro* assay using *L. major* amastigotes, since it is the more relevant form of the parasite for the human host. An *in vivo* model using mice infected with CL would be useful to demonstrate AgNP ability to control skin parasite infection while improving the skin cosmetic outcome.

BIBLIOGRAPHY

1. Catauro, M., Raucci, M. G., de Gaetano, F., & Marotta, A. (2004). Antibacterial and bioactive silver-containing $Na_2O{\cdot}CaO{\cdot}2SiO_2$ glass prepared by sol–gel method. *Journal of Materials Science: Materials in Medicine*, *15*(7), 831–837. https://doi.org/10.1023/B:JMSM.0000032825.51052.00
2. Crabtree, J. H., Burchette, R. J., Siddiqi, R. A., Huen, I. T., Hadnott, L. L., & Fishman, A. (2003). The Efficacy of Silver-Ion Implanted Catheters in Reducing Peritoneal Dialysis-Related Infections. *Peritoneal Dialysis International: Journal of the International Society for Peritoneal Dialysis*, *23*(4), 368–374. https://doi.org/10.1177/089686080302300410
3. Maillard, J.-Y., & Hartemann, P. (2013). Silver as an antimicrobial: facts and gaps in knowledge. *Critical Reviews in Microbiology*, *39*(4), 373–383. https://doi.org/10.3109/1040841X.2012.713323
4. Zhang, X.-F., Liu, Z.-G., Shen, W., & Gurunathan, S. (2016). Silver Nanoparticles: Synthesis, Characterization, Properties, Applications, and Therapeutic Approaches. *International Journal of Molecular Sciences*, *17*(9), 1534. https://doi.org/10.3390/ijms17091534
5. Sotiriou, G. A., & Pratsinis, S. E. (2010). Antibacterial Activity of Nanosilver Ions and Particles. *Environmental Science & Technology*, *44*(14), 5649–5654. https://doi.org/10.1021/es101072s
6. Moreno, E., Schwartz, J., Fernández, C., Sanmartín, C., Nguewa, P., Irache, J. M., & Espuelas, S. (2014). Nanoparticles as multifunctional devices for the topical treatment of cutaneous leishmaniasis. *Expert Opinion on Drug Delivery*, *11*(4), 579–597. https://doi.org/10.1517/17425247.2014.885500
7. Cameron, P., Gaiser, B. K., Bhandari, B., Bartley, P. M., Katzer, F., & Bridle, H. (2016). Silver Nanoparticles Decrease the Viability of *Cryptosporidium parvum* Oocysts. *Applied and Environmental Microbiology*, *82*(2), 431–437. https://doi.org/10.1128/AEM.02806-15
8. Zou, X., Li, P., Lou, J., & Zhang, H. (2017). Surface coating-modulated toxic responses to silver nanoparticles in *Wolffia globosa*. *Aquatic Toxicology*, *189*, 150–158. https://doi.org/10.1016/j.aquatox.2017.06.010
9. Flores-López, L. Z., Espinoza-Gómez, H., & Somanathan, R. (2019). Silver nanoparticles: Electron transfer, reactive oxygen species, oxidative stress, beneficial and toxicological effects. Mini review. *Journal of Applied Toxicology*, *39*(1), 16–26. https://doi.org/10.1002/jat.3654

10. Piao, M. J., Kang, K. A., Lee, I. K., Kim, H. S., Kim, S., Choi, J. Y., Choi, J., & Hyun, J. W. (2011). Silver nanoparticles induce oxidative cell damage in human liver cells through inhibition of reduced glutathione and induction of mitochondria-involved apoptosis. *Toxicology Letters*, *201*(1), 92–100. https://doi.org/10.1016/j.toxlet.2010.12.010
11. Li, Y., Guo, M., Lin, Z., Zhao, M., Xiao, M., Wang, C., Xu, T., Chen, T., & Zhu, B. (2016). Polyethylenimine-functionalized silver nanoparticle-based co-delivery of paclitaxel to induce HepG2 cell apoptosis. *International Journal of Nanomedicine*, *Volume 11*, 6693–6702. https://doi.org/10.2147/IJN.S122666
12. Iravani, S. (2011). Green synthesis of metal nanoparticles using plants. *Green Chemistry*, *13*(10), 2638. https://doi.org/10.1039/c1gc15386b
13. Jamkhande, P. G., Ghule, N. W., Bamer, A. H., & Kalaskar, M. G. (2019). Metal nanoparticles synthesis: An overview on methods of preparation, advantages and disadvantages, and applications. *Journal of Drug Delivery Science and Technology*, *53*, 101174. https://doi.org/10.1016/j.jddst.2019.101174
14. Agnihotri, S., Mukherji, S., & Mukherji, S. (2014). Size-controlled silver nanoparticles synthesized over the range 5–100 nm using the same protocol and their antibacterial efficacy. *RSC Adv.*, *4*(8), 3974–3983. https://doi.org/10.1039/C3RA44507K
15. Pantidos, N. (2014). Biological Synthesis of Metallic Nanoparticles by Bacteria, Fungi and Plants. *Journal of Nanomedicine & Nanotechnology*, *05*(05). https://doi.org/10.4172/2157-7439.1000233
16. Aramwit, P., Bang, N., Ratanavaraporn, J., & Ekgasit, S. (2014). Green synthesis of silk sericin-capped silver nanoparticles and their potent anti-bacterial activity. *Nanoscale Research Letters*, *9*(1), 79. https://doi.org/10.1186/1556-276X-9-79
17. Kumar, R., Roopan, S. M., Prabhakarn, A., Khanna, V. G., & Chakroborty, S. (2012). Agricultural waste *Annona squamosa* peel extract: Biosynthesis of silver nanoparticles. *Spectrochimica Acta Part A: Molecular and Biomolecular Spectroscopy*, *90*, 173–176. https://doi.org/10.1016/j.saa.2012.01.029
18. Roopan, S. M., Bharathi, A., Prabhakarn, A., Abdul Rahuman, A., Velayutham, K., Rajakumar, G., Padmaja, R. D., Lekshmi, M., & Madhumitha, G. (2012). Efficient phyto-synthesis and structural characterization of rutile TiO_2 nanoparticles using *Annona squamosa* peel extract. *Spectrochimica Acta Part A: Molecular and Biomolecular Spectroscopy*, *98*, 86–90. https://doi.org/10.1016/j.saa.2012.08.055
19. Vijayakumar, S., Malaikozhundan, B., Saravanakumar, K., Durán-Lara, E. F., Wang, M.-H., & Vaseeharan, B. (2019). Garlic clove extract assisted silver nanoparticle – Antibacterial, antibiofilm, antihelminthic, anti-inflammatory, anticancer and ecotoxicity assessment. *Journal of Photochemistry and Photobiology B: Biology*, *198*, 111558. https://doi.org/10.1016/j.jphotobiol.2019.111558

20. Song, J. Y., & Kim, B. S. (2009). Rapid biological synthesis of silver nanoparticles using plant leaf extracts. *Bioprocess and Biosystems Engineering*, *32*(1), 79–84. https://doi.org/10.1007/s00449-008-0224-6

21. Vishwanath, R., & Negi, B. (2021). Conventional and green methods of synthesis of silver nanoparticles and their antimicrobial properties. *Current Research in Green and Sustainable Chemistry*, *4*, 100205. https://doi.org/10.1016/j.crgsc.2021.100205

22. Siddiqi, K. S., Husen, A., & Rao, R. A. K. (2018). A review on biosynthesis of silver nanoparticles and their biocidal properties. *Journal of Nanobiotechnology*, *16*(1), 14. https://doi.org/10.1186/s12951-018-0334-5

23. Faria-Silva, C., de Sousa, M., Carvalheiro, M. C., Simões, P., & Simões, S. (2022). Alpha-tomatine and the two sides of the same coin: An anti-nutritional glycoalkaloid with potential in human health. *Food Chemistry*, *391*, 133261. https://doi.org/10.1016/j.foodchem.2022.133261

24. Chaudhary, P., Sharma, A., Singh, B., & Nagpal, A. K. (2018). Bioactivities of phytochemicals present in tomato. *Journal of Food Science and Technology*, *55*(8), 2833–2849. https://doi.org/10.1007/s13197-018-3221-z

25. Tan, H.-L., Thomas-Ahner, J. M., Grainger, E. M., Wan, L., Francis, D. M., Schwartz, S. J., Erdman, J. W., & Clinton, S. K. (2010). Tomato-based food products for prostate cancer prevention: what have we learned? *Cancer and Metastasis Reviews*, *29*(3), 553–568. https://doi.org/10.1007/s10555-010-9246-z

26. Sesso, H. D., Buring, J. E., Norkus, E. P., & Gaziano, J. M. (2004). Plasma lycopene, other carotenoids, and retinol and the risk of cardiovascular disease in women. *The American Journal of Clinical Nutrition*, *79*(1), 47–53. https://doi.org/10.1093/ajcn/79.1.47

27. Agarwal, S., & Rao, A. V. (2000). Tomato lycopene and its role in human health and chronic diseases. *CMAJ : Canadian Medical Association Journal = Journal de l'Association Medicale Canadienne*, *163*(6), 739–744.

28. Chaudhary, A., Harminder, & Singh, V. (2011). A Review on the Taxonomy, Ethnobotany, Chemistry and Pharmacology of *Oroxylum indicum Vent*. *Indian Journal of Pharmaceutical Sciences*, *73*(5), 483. https://doi.org/10.4103/0250-474X.98981

29. Friedman, M., Levin, C. E., Lee, S.-U., Kim, H.-J., Lee, I.-S., Byun, J.-O., & Kozukue, N. (2009). Tomatine-Containing Green Tomato Extracts Inhibit Growth of Human Breast, Colon, Liver, and Stomach Cancer Cells. *Journal of Agricultural and Food Chemistry*, *57*(13), 5727–5733. https://doi.org/10.1021/jf900364j

30. Chao, M.W., Chen, C.H., Chang, Y.L., Teng, C.M., & Pan, S.L. (2012). α-Tomatine-Mediated Anti-Cancer Activity *In Vitro* and *In Vivo* through Cell Cycle- and Caspase-Independent Pathways. *PLoS ONE*, *7*(9), e44093. https://doi.org/10.1371/journal.pone.0044093

31. Friedman, M. (2013). Anticarcinogenic, Cardioprotective, and Other Health Benefits of Tomato Compounds Lycopene, α-Tomatine, and Tomatidine in Pure Form and in Fresh and Processed

Tomatoes. *Journal of Agricultural and Food Chemistry*, *61*(40), 9534–9550. https://doi.org/10.1021/jf402654e

32. Friedman, M., Fitch, T. E., Levin, C. E., & Yokoyama, W. H. (2000). Feeding Tomatoes to Hamsters Reduces their Plasma Low-density Lipoprotein Cholesterol and Triglycerides. *Journal of Food Science*, *65*(5), 897–900. https://doi.org/10.1111/j.1365-2621.2000.tb13608.x
33. Stephen K. Ritter. (2014). A Natural Green Boost For Muscles. *Chemical & Engineering News Archive*, *92*(18), 27–28. https://doi.org/10.1021/cen-09218-scitech1
34. Nepal, B., & J. Stine, K. (2019). Glycoalkaloids: Structure, Properties, and Interactions with Model Membrane Systems. *Processes*, *7*(8), 513. https://doi.org/10.3390/pr7080513
35. Patel, A. H., Sharma, H. P., & Vaishali. (2023). Physiological functions, pharmacological aspects and nutritional importance of green tomato- a future food. *Critical Reviews in Food Science and Nutrition*, 1–29. https://doi.org/10.1080/10408398.2023.2212766
36. Bhat, S. R. (2005). Chlorophyll: The wonder pigment. *Science Repoter*, *42(7)*, 29–32.
37. Mishra, V. K., Kumar Bachheti, R., Husen, A., Mishra, V. K., & Bacheti, R. K. (2011). *Medicinal Uses of Chlorophyll: A Critical Overview*.
38. Prasetyo, B. C., Sugiharti, R. J., Mahendra, I., Halimah, I., Widyasar, E. M., Rusminah, N., & Mustika, I. (2018). Evaluation of Silver Nanoparticles Addition in Periodontal Dressing For Wound Tissue Healing By 99mTc-ciprofloxacin. *Journal of Young Pharmacists*, *11*(1), 17–20. https://doi.org/10.5530/jyp.2019.11.4
39. Kowalczyk, P., Szymczak, M., Maciejewska, M., Laskowski, Ł., Laskowska, M., Ostaszewski, R., Skiba, G., & Franiak-Pietryga, I. (2021). All That Glitters Is Not Silver—A New Look at Microbiological and Medical Applications of Silver Nanoparticles. *International Journal of Molecular Sciences*, *22*(2), 854. https://doi.org/10.3390/ijms22020854
40. Besinis, A., De Peralta, T., & Handy, R. D. (2014). The antibacterial effects of silver, titanium dioxide and silica dioxide nanoparticles compared to the dental disinfectant chlorhexidine on *Streptococcus* mutans using a suite of bioassays. *Nanotoxicology*, *8*(1), 1–16. https://doi.org/10.3109/17435390.2012.742935
41. Lauritano, D., Cura, F., Candotto, V., Gaudio, R. M., Mucchi, D., & Carinci, F. (2015). Evaluation of the efficacy of titanium dioxide with monovalent silver ions covalently linked (TIAB) as an adjunct to scaling and root planing in the management of chronic periodontitis using PCR analysis: A microbiological study. *Journal of Biological Regulators and Homeostatic Agents*, *29*(3 Suppl 1), 127–130.
42. Garzon, S., Laganà, A. S., Ghezzi, F., & Cassarin, J. (2019). Effects of Microcrystalline Titanium Dioxide With Covalently Linked Monovalent Silver Ions on Complications After Total Hysterectomy (ISTIAB-0).
43. Murina, F., & Vicariotto, F. (2015). Vulvar Dermatoses: Effect of a Synergistic Treatment with a Moisturizing and Healing Product on the Course of the Disease. *Open Journal of Obstetrics and Gynecology*, *05*(05), 239–243. https://doi.org/10.4236/ojog.2015.55035

44. Bharti, A., Singh, S., Meena, V. K., & Goyal, N. (2016). Structural Characterization of Silver-Hydroxyapatite Nanocomposite: A Bone Repair Biomaterial. *Materials Today: Proceedings*, *3*(6), 2113–2120. https://doi.org/10.1016/j.matpr.2016.04.116

45. Qing, Y., Cheng, L., Li, R., Liu, G., Zhang, Y., Tang, X., Wang, J., Liu, H., & Qin, Y. (2018). Potential antibacterial mechanism of silver nanoparticles and the optimization of orthopedic implants by advanced modification technologies. *International Journal of Nanomedicine*, *Volume 13*, 3311–3327. https://doi.org/10.2147/IJN.S165125

46. Aurore, V., Caldana, F., Blanchard, M., Kharoubi Hess, S., Lannes, N., Mantel, P.-Y., Filgueira, L., & Walch, M. (2018). Silver-nanoparticles increase bactericidal activity and radical oxygen responses against bacterial pathogens in human osteoclasts. *Nanomedicine: Nanotechnology, Biology and Medicine*, *14*(2), 601–607. https://doi.org/10.1016/j.nano.2017.11.006

47. Kundu, N., Mukherjee, D., Maiti, T. K., & Sarkar, N. (2017). Protein-Guided Formation of Silver Nanoclusters and Their Assembly with Graphene Oxide as an Improved Bioimaging Agent with Reduced Toxicity. *The Journal of Physical Chemistry Letters*, *8*(10), 2291–2297. https://doi.org/10.1021/acs.jpclett.7b00600

48. Xiong, H., Zheng, H., Wang, W., Liang, J., Wen, W., Zhang, X., & Wang, S. (2016). A convenient purification method for silver nanoclusters and its applications in fluorescent pH sensors for bacterial monitoring. *Biosensors and Bioelectronics*, *86*, 164–168. https://doi.org/10.1016/j.bios.2016.06.038

49. Geng, Z., Wang, R., Zhuo, X., Li, Z., Huang, Y., Ma, L., Cui, Z., Zhu, S., Liang, Y., Liu, Y., Bao, H., Li, X., Huo, Q., Liu, Z., & Yang, X. (2017). Incorporation of silver and strontium in hydroxyapatite coating on titanium surface for enhanced antibacterial and biological properties. *Materials Science and Engineering: C*, *71*, 852–861. https://doi.org/10.1016/j.msec.2016.10.079

50. Syafiuddin, A., Salmiati, S., Hadibarata, T., Kueh, A. B. H., Salim, M. R., & Zaini, M. A. A. (2018). Silver Nanoparticles in the Water Environment in Malaysia: Inspection, characterization, removal, modeling, and future perspective. *Scientific Reports*, *8*(1), 986. https://doi.org/10.1038/s41598-018-19375-1

51. Que, Z. G., Torres, J. G. T., Vidal, H. P., Rocha, M. A. L., Pérez, J. C. A., López, I. C., Romero, D. D. L. C., Reyna, A. E. E. D. L. M., Sosa, J. G. P., Pavón, A. A. S., & Hernández, J. S. F. (2018). Application of Silver Nanoparticles for Water Treatment. In *Silver Nanoparticles - Fabrication, Characterization and Applications*. InTech. https://doi.org/10.5772/intechopen.74675

52. Fiorati, A., Bellingeri, A., Punta, C., Corsi, I., & Venditti, I. (2020). Silver Nanoparticles for Water Pollution Monitoring and Treatments: Ecosafety Challenge and Cellulose-Based Hybrids Solution. *Polymers*, *12*(8), 1635. https://doi.org/10.3390/polym12081635

53. Istiqola, A., & Syafiuddin, A. (2020). A review of silver nanoparticles in food packaging technologies: Regulation, methods, properties, migration, and future challenges. *Journal of the Chinese Chemical Society*, *67*(11), 1942–1956. https://doi.org/10.1002/jccs.202000179

54. Montes-Hernandez, G., Di Girolamo, M., Sarret, G., Bureau, S., Fernandez-Martinez, A., Lelong, C., & Eymard Vernain, E. (2021). *In Situ* Formation of Silver Nanoparticles (Ag-NPs) onto Textile Fibers. *ACS Omega*, *6*(2), 1316–1327. https://doi.org/10.1021/acsomega.0c04814

55. Almayouf, M. A., El-khadragy, M., Awad, M. A., & Alolayan, E. M. (2020). The effects of silver nanoparticles biosynthesized using fig and olive extracts on cutaneous leishmaniasis-induced inflammation in female balb/c mice. *Bioscience Reports*, *40*(12). https://doi.org/10.1042/BSR20202672

56. Shakeel, M., Kiani, M. H., Sarwar, H. S., Akhtar, S., Rauf, A., Ibrahim, I. M., Ajalli, N., Shahnaz, G., Rahdar, A., & Díez-Pascual, A. M. (2023). Emulgel-loaded mannosylated thiolated chitosan-coated silver nanoparticles for the treatment of cutaneous leishmaniasis. *International Journal of Biological Macromolecules*, *227*, 1293–1304. https://doi.org/10.1016/j.ijbiomac.2022.11.326

57. Shnawa, B. H., Jalil, P. J., & Swar, S. O. (2023). Greener Nanoparticles: Potential Alternative Approach to Fight Protozoal Diseases. In *International Journal of Agriculture and Biology* (Vol. 30, Issue 3, pp. 189–199). Friends Science Publishers. https://doi.org/10.17957/IJAB/15.2075

58. Mohammadi, M., Zaki, L., KarimiPourSaryazdi, A., Tavakoli, P., Tavajjohi, A., Poursalehi, R., Delavari, H., & Ghaffarifar, F. (2021). Efficacy of green synthesized silver nanoparticles via ginger rhizome extract against *Leishmania major in vitro*. *PLOS ONE*, *16*(8), e0255571. https://doi.org/10.1371/journal.pone.0255571

59. Alti, D., Veeramohan Rao, M., Rao, D. N., Maurya, R., & Kalangi, S. K. (2020). Gold–Silver Bimetallic Nanoparticles Reduced with Herbal Leaf Extracts Induce ROS-Mediated Death in Both Promastigote and Amastigote Stages of *Leishmania donovani*. *ACS Omega*, *5*(26), 16238–16245. https://doi.org/10.1021/acsomega.0c02032

60. Alemzadeh, E., Karamian, M., Abedi, F., & Hanafi-Bojd, M. Y. (2022). Topical treatment of cutaneous leishmaniasis lesions using quercetin/ Artemisia-capped silver nanoparticles ointment: Modulation of inflammatory response. *Acta Tropica*, *228*, 106325. https://doi.org/10.1016/j.actatropica.2022.106325

61. World Health Organization. (2023, January 13). *Leishmaniasis*.

62. Mokni, M. (2019). Leishmanioses cutanées. *Annales de Dermatologie et de Vénéréologie*, *146*(3), 232–246. https://doi.org/10.1016/j.annder.2019.02.002

63. Sousa-Batista, A., & Rossi-Bergmann, B. (2018). Nanomedicines for Cutaneous Leishmaniasis. In *Leishmaniases as Re-emerging Diseases*. InTech. https://doi.org/10.5772/intechopen.75750

64. Van der Auwera, G., Davidsson, L., Buffet, P., Ruf, M. T., Gramiccia, M., Varani, S., Chicharro, C., Bart, A., Harms, G., Chiodini, P. L., Brekke, H., Robert-Gangneux, F., Cortes, S., Verweij, J. J., Scarabello, A., Karlsson Söbirk, S., Guéry, R., van Henten, S., Di Muccio, T., Carra, E., … LeishMan Surveillance Network members who contributed to this article (in addition to authors above) (2022). Surveillance of leishmaniasis cases from 15 European centres, 2014 to 2019: a retrospective analysis. *Eurosurveillance*, *27*(4). https://doi.org/10.2807/1560-7917.ES.2022.27.4.2002028

65. Kevric, I., Cappel, M. A., & Keeling, J. H. (2015). New World and Old World *Leishmania* Infections. *Dermatologic Clinics*, *33*(3), 579–593. https://doi.org/10.1016/j.det.2015.03.018

66. Copeland, N. K., & Aronson, N. E. (2015). Leishmaniasis: Treatment updates and clinical practice guidelines review. *Current Opinion in Infectious Diseases*, *28*(5), 426–437. https://doi.org/10.1097/QCO.0000000000000194

67. Bailey, M. S., & Lockwood, D. N. J. (2007). Cutaneous leishmaniasis. *Clinics in Dermatology*, *25*(2), 203–211. https://doi.org/10.1016/j.clindermatol.2006.05.008

68. Chagas, A. C., Oliveira, F., Debrabant, A., Valenzuela, J. G., Ribeiro, J. M. C., & Calvo, E. (2014). Lundep, a Sand Fly Salivary Endonuclease Increases *Leishmania* Parasite Survival in Neutrophils and Inhibits XIIa Contact Activation in Human Plasma. *PLoS Pathogens*, *10*(2), e1003923. https://doi.org/10.1371/journal.ppat.1003923

69. Pearson, R. D., Wheeler, D. A., Harrison, L. H., & Kay, H. D. (1983). The Immunobiology of Leishmaniasis. *Clinical Infectious Diseases*, *5*(5), 907–927. https://doi.org/10.1093/clinids/5.5.907

70. Franco, L. H., Beverley, S. M., & Zamboni, D. S. (2012). Innate Immune Activation and Subversion of Mammalian Functions by *Leishmania* Lipophosphoglycan. *Journal of Parasitology Research*, *2012*, 1–11. https://doi.org/10.1155/2012/165126

71. Ng, V. H., Cox, J. S., Sousa, A. O., MacMicking, J. D., & McKinney, J. D. (2004). Role of KatG catalase-peroxidase in mycobacterial pathogenesis: countering the phagocyte oxidative burst. *Molecular Microbiology*, *52*(5), 1291–1302. https://doi.org/10.1111/j.1365-2958.2004.04078.x

72. Rossi, M., & Fasel, N. (2018). How to master the host immune system? Leishmania parasites have the solutions! *International Immunology*, *30*(3), 103–111. https://doi.org/10.1093/intimm/dxx075

73. Panday, A., Sahoo, M. K., Osorio, D., & Batra, S. (2015). NADPH oxidases: an overview from structure to innate immunity-associated pathologies. *Cellular & Molecular Immunology*, *12*(1), 5–23. https://doi.org/10.1038/cmi.2014.89

74. Gaur, U., Roberts, S. C., Dalvi, R. P., Corraliza, I., Ullman, B., & Wilson, M. E. (2007). An Effect of Parasite-Encoded Arginase on the Outcome of Murine Cutaneous Leishmaniasis. *The Journal of Immunology*, *179*(12), 8446–8453. https://doi.org/10.4049/jimmunol.179.12.8446

75. Uliana, S. R. B., Trinconi, C. T., & Coelho, A. C. (2018). Chemotherapy of leishmaniasis: present challenges. *Parasitology*, *145*(4), 464–480. https://doi.org/10.1017/S0031182016002523

76. Jain, K., & Jain, N. K. (2013). Novel therapeutic strategies for treatment of visceral leishmaniasis. *Drug Discovery Today*, *18*(23–24), 1272–1281. https://doi.org/10.1016/j.drudis.2013.08.005

77. Shahnaz, G., Sarwar, H. S., & Yasinzai, M. (2018). Crossing Biological Barriers for Leishmaniasis Therapy: From Nanomedicinal Targeting Perspective. In *Leishmaniases as Re-emerging Diseases*. InTech. https://doi.org/10.5772/intechopen.75911

78. Monge-Maillo, B., & Lopez-Velez, R. (2015). Miltefosine for Visceral and Cutaneous Leishmaniasis: Drug Characteristics and Evidence-Based Treatment Recommendations. *Clinical Infectious Diseases*. https://doi.org/10.1093/cid/civ004

79. Dorlo, T. P. C., Balasegaram, M., Beijnen, J. H., & de Vries, P. J. (2012). Miltefosine: a review of its pharmacology and therapeutic efficacy in the treatment of leishmaniasis. *Journal of Antimicrobial Chemotherapy*, *67*(11), 2576–2597. https://doi.org/10.1093/jac/dks275

80. Bern, C., Adler-Moore, J., Berenguer, J., Boelaert, M., Boer, M. den, Davidson, R. N., Figueras, C., Gradoni, L., Kafetzis, D. A., Ritmeijer, K., Rosenthal, E., Royce, C., Russo, R., Sundar, S., & Alvar, J. (2006). Reviews Of Anti-infective Agents: Liposomal Amphotericin B for the Treatment of Visceral Leishmaniasis. *Clinical Infectious Diseases*, *43*(7), 917–924. https://doi.org/10.1086/507530

81. Gustafson, H. H., Holt-Casper, D., Grainger, D. W., & Ghandehari, H. (2015). Nanoparticle uptake: The phagocyte problem. *Nano Today*, *10*(4), 487–510. https://doi.org/10.1016/j.nantod.2015.06.006

82. Zhou, Y., Messier, N., Ouellette, M., Rosen, B. P., & Mukhopadhyay, R. (2004). *Leishmania major* LmACR2 Is a Pentavalent Antimony Reductase That Confers Sensitivity to the Drug Pentostam. *Journal of Biological Chemistry*, *279*(36), 37445–37451. https://doi.org/10.1074/jbc.M404383200

83. Denton, H., McGregor, J. C., & Coombs, G. H. (2004). Reduction of anti-leishmanial pentavalent antimonial drugs by a parasite-specific thiol-dependent reductase, TDR1. *Biochemical Journal*, *381*(2), 405–412. https://doi.org/10.1042/BJ20040283

84. dos Santos Ferreira, C., Silveira Martins, P., Demicheli, C., Brochu, C., Ouellette, M., & Frézard, F. (2003). Thiol-induced reduction of antimony(V) into antimony(III): A comparative study with trypanothione, cysteinyl-glycine, cysteine and glutathione. *BioMetals*, *16*(3), 441–446. https://doi.org/10.1023/A:1022823605068

85. Maharjan, M., Madhubala, R., Chatterjee, M., & Singh, S. (2008). Role of Aquaglyceroporin (AQP1) Gene and Drug Uptake in Antimony-resistant Clinical Isolates of *Leishmania donovani*. *The American Journal of Tropical Medicine and Hygiene*, *79*(1), 69–75. https://doi.org/10.4269/ajtmh.2008.79.69

86. Mandal, G., Mandal, S., Sharma, M., Charret, K. S., Papadopoulou, B., Bhattacharjee, H., & Mukhopadhyay, R. (2015). Species-Specific Antimonial Sensitivity in *Leishmania* Is Driven by Post-Transcriptional Regulation of AQP1. *PLOS Neglected Tropical Diseases*, *9*(2), e0003500. https://doi.org/10.1371/journal.pntd.0003500

87. Rugani, J. N., Gontijo, C. M. F., Frézard, F., Soares, R. P., & Monte-Neto, R. L. do. (2019). Antimony resistance in *Leishmania (Viannia) braziliensis* clinical isolates from atypical lesions associates with increased ARM56/ARM58 transcripts and reduced drug uptake. *Memórias Do Instituto Oswaldo Cruz*, *114*. https://doi.org/10.1590/0074-02760190111

88. Wijnant, G.-J., Dumetz, F., Dirkx, L., Bulté, D., Cuypers, B., Van Bocxlaer, K., & Hendrickx, S. (2022). Tackling Drug Resistance and Other Causes of Treatment Failure in Leishmaniasis. *Frontiers in Tropical Diseases*, *3*. https://doi.org/10.3389/fitd.2022.837460

89. Roatt, B. M., Aguiar-Soares, R. D. de O., Coura-Vital, W., Ker, H. G., Moreira, N. das D., Vitoriano-Souza, J., Giunchetti, R. C., Carneiro, C. M., & Reis, A. B. (2014). Immunotherapy and Immunochemotherapy in Visceral Leishmaniasis: Promising Treatments for this Neglected Disease. *Frontiers in Immunology*, *5*. https://doi.org/10.3389/fimmu.2014.00272

90. Purkait, B., Kumar, A., Nandi, N., Sardar, A. H., Das, S., Kumar, S., Pandey, K., Ravidas, V., Kumar, M., De, T., Singh, D., & Das, P. (2012). Mechanism of Amphotericin B Resistance in Clinical Isolates of *Leishmania donovani*. *Antimicrobial Agents and Chemotherapy*, *56*(2), 1031–1041. https://doi.org/10.1128/AAC.00030-11

91. Maarouf, M., de Kouchkovsky, Y., Brown, S., Petit, P. X., & Robert-Gero, M. (1997). *In Vivo* Interference of Paromomycin with Mitochondrial Activity of *Leishmania*. *Experimental Cell Research*, *232*(2), 339–348. https://doi.org/10.1006/excr.1997.3500

92. Maarouf, M., Lawrence, F., Croft, S. L., & Robert-Gero, M. (1995). Ribosomes of *Leishmania* are a target for the aminoglycosides. *Parasitology Research*, *81*(5), 421–425. https://doi.org/10.1007/BF00931504

93. Chawla, B., Jhingran, A., Panigrahi, A., Stuart, K. D., & Madhubala, R. (2011). Paromomycin Affects Translation and Vesicle-Mediated Trafficking as Revealed by Proteomics of Paromomycin – Susceptible–Resistant *Leishmania donovani*. *PLoS ONE*, *6*(10), e26660. https://doi.org/10.1371/journal.pone.0026660

94. Bhandari, V., Sundar, S., Dujardin, J. C., & Salotra, P. (2014). Elucidation of Cellular Mechanisms Involved in Experimental Paromomycin Resistance in *Leishmania donovani*. *Antimicrobial Agents and Chemotherapy*, *58*(5), 2580–2585. https://doi.org/10.1128/AAC.01574-13

95. Jhingran, A., Chawla, B., Saxena, S., Barrett, M. P., & Madhubala, R. (2009). Paromomycin: Uptake and resistance in *Leishmania donovani*. *Molecular and Biochemical Parasitology*, *164*(2), 111–117. https://doi.org/10.1016/j.molbiopara.2008.12.007

96. Rakotomanga, M., Blanc, S., Gaudin, K., Chaminade, P., & Loiseau, P. M. (2007). Miltefosine Affects Lipid Metabolism in *Leishmania donovani* Promastigotes. *Antimicrobial Agents and Chemotherapy*, *51*(4), 1425–1430. https://doi.org/10.1128/AAC.01123-06

97. Luque-Ortega, J. R., & Rivas, L. (2007). Miltefosine (Hexadecylphosphocholine) Inhibits Cytochrome c Oxidase in *Leishmania donovani* Promastigotes. *Antimicrobial Agents and Chemotherapy*, *51*(4), 1327–1332. https://doi.org/10.1128/AAC.01415-06

98. Pinto-Martinez, A. K., Rodriguez-Durán, J., Serrano-Martin, X., Hernandez-Rodriguez, V., & Benaim, G. (2018). Mechanism of Action of Miltefosine on *Leishmania donovani* Involves the Impairment of Acidocalcisome Function and the Activation of the Sphingosine-Dependent Plasma Membrane Ca^{2+} Channel. *Antimicrobial Agents and Chemotherapy*, *62*(1). https://doi.org/10.1128/AAC.01614-17

99. Wadhone, P., Maiti, M., Agarwal, R., Kamat, V., Martin, S., & Saha, B. (2009). Miltefosine Promotes IFN-γ-Dominated Anti-Leishmanial Immune Response. *The Journal of Immunology*, *182*(11), 7146–7154. https://doi.org/10.4049/jimmunol.0803859

100. Mondelaers, A., Sanchez-Cañete, M. P., Hendrickx, S., Eberhardt, E., Garcia-Hernandez, R., Lachaud, L., Cotton, J., Sanders, M., Cuypers, B., Imamura, H., Dujardin, J.-C., Delputte, P., Cos, P., Caljon, G., Gamarro, F., Castanys, S., & Maes, L. (2016). Genomic and Molecular Characterization of Miltefosine Resistance in *Leishmania infantum* Strains with Either Natural or Acquired Resistance through Experimental Selection of Intracellular Amastigotes. *PLOS ONE*, *11*(4), e0154101. https://doi.org/10.1371/journal.pone.0154101

101. Muller, R., Petersen, R., Hommoss, A., & Pardeike, J. (2007). Nanostructured lipid carriers (NLC) in cosmetic dermal products. *Advanced Drug Delivery Reviews*, *59*(6), 522–530. https://doi.org/10.1016/j.addr.2007.04.012

102. Müller, R. H., Radtke, M., & Wissing, S. A. (2002). Nanostructured lipid matrices for improved microencapsulation of drugs. *International Journal of Pharmaceutics*, *242*(1–2), 121–128. https://doi.org/10.1016/S0378-5173(02)00180-1

103. Zhuang, C.-Y., Li, N., Wang, M., Zhang, X.-N., Pan, W.-S., Peng, J.-J., Pan, Y.-S., & Tang, X. (2010). Preparation and characterization of vinpocetine loaded nanostructured lipid carriers (NLC) for improved oral bioavailability. *International Journal of Pharmaceutics*, *394*(1–2), 179–185. https://doi.org/10.1016/j.ijpharm.2010.05.005

104. Vieira, A. C., Magalhães, J., Rocha, S., Cardoso, M. S., Santos, S. G., Borges, M., Pinheiro, M., & Reis, S. (2017). Targeted macrophages delivery of rifampicin-loaded lipid nanoparticles to improve tuberculosis treatment. *Nanomedicine*, *12*(24), 2721–2736. https://doi.org/10.2217/nnm-2017-0248

105. Hachem, R. Y., Boktour, M. R., Hanna, H. A., Husni, R. N., Torres, H. A., Afif, C., Kontoyiannis, D. P., & Raad, I. I. (2008). Amphotericin B lipid complex versus liposomal amphotericin B monotherapy for invasive aspergillosis in patients with hematologic malignancy. *Cancer*, *112*(6), 1282–1287. https://doi.org/10.1002/cncr.23311

106. Chan, M. M.-Y., & Fong, D. (1990). Inhibition of Leishmanias But Not Host Macrophages by the Antitubulin Herbicide Trifluralin. *Science*, *249*(4971), 924–926. https://doi.org/10.1126/science.2392684

107. Esteves, M. A., Fragiadaki, I., Lopes, R., Scoulica, E., & Cruz, M. E. M. (2010). Synthesis and biological evaluation of trifluralin analogues as antileishmanial agents. *Bioorganic & Medicinal Chemistry*, *18*(1), 274–281. https://doi.org/10.1016/j.bmc.2009.10.059

108. Benbow, J. W., Bernberg, E. L., Korda, A., & Mead, J. R. (1998). Synthesis and Evaluation of Dinitroanilines for Treatment of Cryptosporidiosis. *Antimicrobial Agents and Chemotherapy*, *42*(2), 339–343. https://doi.org/10.1128/AAC.42.2.339

109. Godinho, J. L. P., Georgikopoulou, K., Calogeropoulou, T., de Souza, W., & Rodrigues, J. C. F. (2013). A novel alkyl phosphocholine-dinitroaniline hybrid molecule exhibits biological activity in vitro

against *Leishmania amazonensis*. *Experimental Parasitology*, *135*(1), 153–165. https://doi.org/10.1016/j.exppara.2013.06.015

110. Carvalheiro, M., Jorge, J., Eleutério, C., Pinhal, A. F., Sousa, A. C., Morais, J. G., & Cruz, M. E. M. (2009). Trifluralin liposomal formulations active against *Leishmania donovani* infections. *European Journal of Pharmaceutics and Biopharmaceutics*, *71*(2), 292–296. https://doi.org/10.1016/j.ejpb.2008.08.001
111. Pedras, B., Salema-Oom, M., Sá-Nogueira, I., Simões, P., Paiva, A., & Barreiros, S. (2017). Valorization of white wine grape pomace through application of subcritical water: Analysis of extraction, hydrolysis, and biological activity of the extracts obtained. *The Journal of Supercritical Fluids*, *128*, 138–144. https://doi.org/10.1016/j.supflu.2017.05.020
112. Singleton, V. L., & Rossi, J. A. (1965). Colorimetry of Total Phenolics with Phosphomolybdic-Phosphotungstic Acid Reagents. *American Journal of Enology and Viticulture*, *16*(3), 144–158. https://doi.org/10.5344/ajev.1965.16.3.144
113. Jayachandran, P., Ilango, S., Suseela, V., Nirmaladevi, R., Shaik, M. R., Khan, M., Khan, M., & Shaik, B. (2023). Green Synthesized Silver Nanoparticle-Loaded Liposome-Based Nanoarchitectonics for Cancer Management: In Vitro Drug Release Analysis. *Biomedicines*, *11*(1). https://doi.org/10.3390/biomedicines11010217
114. Wang, H., Agrawal, A., Wang, Y., Crawford, D. W., Siler, Z. D., Peterson, M. L., Woofter, R. T., Labib, M., Shin, H. Y., Baumann, A. P., & Phillips, K. S. (2021). An ex vivo model of medical device-mediated bacterial skin translocation. *Scientific Reports*, *11*(1), 5746. https://doi.org/10.1038/s41598-021-84826-1
115. Ghosh, P., Fawcett, D., Sharma, S., & Poinern, G. (2017). Production of High-Value Nanoparticles via Biogenic Processes Using Aquacultural and Horticultural Food Waste. *Materials*, *10*(8), 852. https://doi.org/10.3390/ma10080852
116. Ayad, Z. M., Ibrahim, O. M. S., & Omar, L. W. (2019). Biosynthesis and Characterization of Silver Nanoparticles by *Silybum marianum* (silymarin) Fruit Extract. *Advances in Animal and Veterinary Sciences*, *7*(2). https://doi.org/10.17582/journal.aavs/2019/7.2.122.130
117. Mehrdel, B., & Aziz, A. A. (2018). The Sensitivity of Surface Plasmon Resonance Damping for Colloidal Silver Nanoparticles. *Journal of Physics: Conference Series*, *1083*, 012042. https://doi.org/10.1088/1742-6596/1083/1/012042
118. Uchechi, O., Ogbonna, J. D. N., & Attama, A. A. (2014). Nanoparticles for Dermal and Transdermal Drug Delivery. In *Application of Nanotechnology in Drug Delivery*. InTech. https://doi.org/10.5772/58672
119. Samberg, M. E., Oldenburg, S. J., & Monteiro-Riviere, N. A. (2010). Evaluation of Silver Nanoparticle Toxicity in Skin *in Vivo* and Keratinocytes *in Vitro*. *Environmental Health Perspectives*, *118*(3), 407–413. https://doi.org/10.1289/ehp.0901398

120. Tak, Y. K., Pal, S., Naoghare, P. K., Rangasamy, S., & Song, J. M. (2015). Shape-Dependent Skin Penetration of Silver Nanoparticles: Does It Really Matter? *Scientific Reports*, *5*(1), 16908. https://doi.org/10.1038/srep16908

121. Clogston, J. D., & Patri, A. K. (2011). *Zeta Potential Measurement* (pp. 63–70). https://doi.org/10.1007/978-1-60327-198-1_6

122. Vera-Nuñez, L. D. C., Cornejo-Ruiz, J. O., Arenas-Chávez, C. A., de Hollanda, L. M., Alvarez-Risco, A., Del-Aguila-Arcentales, S., Davies, N. M., Yáñez, J. A., & Vera-Gonzales, C. (2022). Green Synthesis of a Novel Silver Nanoparticle Conjugated with *Thelypteris glandulosolanosa* (Raqui-Raqui): Preliminary Characterization and Anticancer Activity. *Processes*, *10*(7), 1308. https://doi.org/10.3390/pr10071308

123. Saha, P., Mahiuddin, Md., Islam, A. B. M. N., & Ochiai, B. (2021). Biogenic Synthesis and Catalytic Efficacy of Silver Nanoparticles Based on Peel Extracts of *Citrus macroptera* Fruit. *ACS Omega*, *6*(28), 18260–18268. https://doi.org/10.1021/acsomega.1c02149

124. Liu, H., Zhang, H., Wang, J., & Wei, J. (2020). Effect of temperature on the size of biosynthesized silver nanoparticle: Deep insight into microscopic kinetics analysis. *Arabian Journal of Chemistry*, *13*(1), 1011–1019. https://doi.org/10.1016/j.arabjc.2017.09.004

125. Philip, D. (2009). Biosynthesis of Au, Ag and Au–Ag nanoparticles using edible mushroom extract. *Spectrochimica Acta Part A: Molecular and Biomolecular Spectroscopy*, *73*(2), 374–381. https://doi.org/10.1016/j.saa.2009.02.037

126. Veerasamy, R., Xin, T. Z., Gunasagaran, S., Xiang, T. F. W., Yang, E. F. C., Jeyakumar, N., & Dhanaraj, S. A. (2011). Biosynthesis of silver nanoparticles using mangosteen leaf extract and evaluation of their antimicrobial activities. *Journal of Saudi Chemical Society*, *15*(2), 113–120. https://doi.org/10.1016/j.jscs.2010.06.004

127. Handayani, W., Ningrum, A. S., & Imawan, C. (2020). The Role of pH in Synthesis Silver Nanoparticles Using *Pometia pinnata* (Matoa) Leaves Extract as Bioreductor. *Journal of Physics: Conference Series*, *1428*(1), 012021. https://doi.org/10.1088/1742-6596/1428/1/012021

128. Ider, M., Abderrafi, K., Eddahbi, A., Ouaskit, S., & Kassiba, A. (2017). Silver Metallic Nanoparticles with Surface Plasmon Resonance: Synthesis and Characterizations. *Journal of Cluster Science*, *28*(3), 1051–1069. https://doi.org/10.1007/s10876-016-1080-1

129. Paramelle, D., Sadovoy, A., Gorelik, S., Free, P., Hobley, J., & Fernig, D. G. (2014). A rapid method to estimate the concentration of citrate capped silver nanoparticles from UV-visible light spectra. *The Analyst*, *139*(19), 4855. https://doi.org/10.1039/C4AN00978A

130. Firoozi, S., Jamzad, M., & Yari, M. (2016). Biologically synthesized silver nanoparticles by aqueous extract of *Satureja intermedia* C.A. Mey and the evaluation of total phenolic and flavonoid contents and antioxidant activity. *Journal of Nanostructure in Chemistry*, *6*(4), 357–364. https://doi.org/10.1007/s40097-016-0207-0

131. Mittal, A. K., Bhaumik, J., Kumar, S., & Banerjee, U. C. (2014). Biosynthesis of silver nanoparticles: Elucidation of prospective mechanism and therapeutic potential. *Journal of Colloid and Interface Science*, *415*, 39–47. https://doi.org/10.1016/j.jcis.2013.10.018

132. Simon, S., Sibuyi, N. R. S., Fadaka, A. O., Meyer, M., Madiehe, A. M., & du Preez, M. G. (2021). The antimicrobial activity of biogenic silver nanoparticles synthesized from extracts of Red and Green European pear cultivars. *Artificial Cells, Nanomedicine, and Biotechnology*, *49*(1), 613–624. https://doi.org/10.1080/21691401.2021.1980884

133. Khane, Y., Benouis, K., Albukhaty, S., Sulaiman, G. M., Abomughaid, M. M., Al Ali, A., Aouf, D., Fenniche, F., Khane, S., Chaibi, W., Henni, A., Bouras, H. D., & Dizge, N. (2022). Green Synthesis of Silver Nanoparticles Using Aqueous *Citrus limon* Zest Extract: Characterization and Evaluation of Their Antioxidant and Antimicrobial Properties. *Nanomaterials*, *12*(12), 2013. https://doi.org/10.3390/nano12122013

134. Singh, T., Jyoti, K., Patnaik, A., Singh, A., Chauhan, R., & Chandel, S. S. (2017). Biosynthesis, characterization and antibacterial activity of silver nanoparticles using an endophytic fungal supernatant of *Raphanus sativus*. *Journal of Genetic Engineering and Biotechnology*, *15*(1), 31–39. https://doi.org/10.1016/j.jgeb.2017.04.005

135. De Muylder, G., Ang, K. K. H., Chen, S., Arkin, M. R., Engel, J. C., & McKerrow, J. H. (2011). A Screen against *Leishmania* Intracellular Amastigotes: Comparison to a Promastigote Screen and Identification of a Host Cell-Specific Hit. *PLoS Neglected Tropical Diseases*, *5*(7), e1253. https://doi.org/10.1371/journal.pntd.0001253

136. Fanti, J. R., Tomiotto-Pellissier, F., Miranda-Sapla, M. M., Cataneo, A. H. D., Andrade, C. G. T. de J., Panis, C., Rodrigues, J. H. da S., Wowk, P. F., Kuczera, D., Costa, I. N., Nakamura, C. V., Nakazato, G., Durán, N., Pavanelli, W. R., & Conchon-Costa, I. (2018). Biogenic silver nanoparticles inducing *Leishmania amazonensis* promastigote and amastigote death in vitro. *Acta Tropica*, *178*, 46–54. https://doi.org/10.1016/j.actatropica.2017.10.027

137. Moulton, M. C., Braydich-Stolle, L. K., Nadagouda, M. N., Kunzelman, S., Hussain, S. M., & Varma, R. S. (2010). Synthesis, characterization and biocompatibility of “green” synthesized silver nanoparticles using tea polyphenols. *Nanoscale*, *2*(5), 763. https://doi.org/10.1039/c0nr00046a

138. Khan, A. A., Alanazi, A. M., Alsaif, N., Wani, T. A., & Bhat, M. A. (2021). Pomegranate peel induced biogenic synthesis of silver nanoparticles and their multifaceted potential against intracellular pathogen and cancer. *Saudi Journal of Biological Sciences*, *28*(8), 4191–4200. https://doi.org/10.1016/j.sjbs.2021.06.022

139. Radzig, M. A., Nadtochenko, V. A., Koksharova, O. A., Kiwi, J., Lipasova, V. A., & Khmel, I. A. (2013). Antibacterial effects of silver nanoparticles on gram-negative bacteria: Influence on the growth and biofilms formation, mechanisms of action. *Colloids and Surfaces B: Biointerfaces*, *102*, 300–306. https://doi.org/10.1016/j.colsurfb.2012.07.039

140. Cavassin, E. D., de Figueiredo, L. F. P., Otoch, J. P., Seckler, M. M., de Oliveira, R. A., Franco, F. F., Marangoni, V. S., Zucolotto, V., Levin, A. S. S., & Costa, S. F. (2015). Comparison of methods to

detect the in vitro activity of silver nanoparticles (AgNP) against multidrug resistant bacteria. *Journal of Nanobiotechnology*, *13*(1), 64. https://doi.org/10.1186/s12951-015-0120-6

141. Qing, Y., Cheng, L., Li, R., Liu, G., Zhang, Y., Tang, X., Wang, J., Liu, H., & Qin, Y. (2018). Potential antibacterial mechanism of silver nanoparticles and the optimization of orthopedic implants by advanced modification technologies. *International Journal of Nanomedicine*, *Volume 13*, 3311–3327. https://doi.org/10.2147/IJN.S165125
142. Chatterjee, T., Chatterjee, B. K., Majumdar, D., & Chakrabarti, P. (2015). Antibacterial effect of silver nanoparticles and the modeling of bacterial growth kinetics using a modified Gompertz model. *Biochimica et Biophysica Acta (BBA) - General Subjects*, *1850*(2), 299–306. https://doi.org/10.1016/j.bbagen.2014.10.022
143. Bruna, T., Maldonado-Bravo, F., Jara, P., & Caro, N. (2021). Silver Nanoparticles and Their Antibacterial Applications. *International Journal of Molecular Sciences*, *22*(13), 7202. https://doi.org/10.3390/ijms22137202
144. Wang, H., Agrawal, A., Wang, Y., Crawford, D. W., Siler, Z. D., Peterson, M. L., Woofter, R. T., Labib, M., Shin, H. Y., Baumann, A. P., & Phillips, K. S. (2021). An *ex vivo* model of medical device-mediated bacterial skin translocation. *Scientific Reports*, *11*(1), 5746. https://doi.org/10.1038/s41598-021-84826-1
145. Ansell, D. M., Campbell, L., Thomason, H. A., Brass, A., & Hardman, M. J. (2014). A statistical analysis of murine incisional and excisional acute wound models. *Wound Repair and Regeneration*, *22*(2), 281–287. https://doi.org/10.1111/wrr.12148
146. Gupta, P., & Garg, S. (2002). Recent Advances in Semisolid Dosage Forms for Dermatological Application. *Pharmaceutical Technology*.
147. Marto, J., Neves, Â., Gonçalves, L., Pinto, P., Almeida, C., & Simões, S. (2018). Rice Water: A Traditional Ingredient with Anti-Aging Efficacy. *Cosmetics*, *5*(2), 26. https://doi.org/10.3390/cosmetics5020026

A
APPENDIX

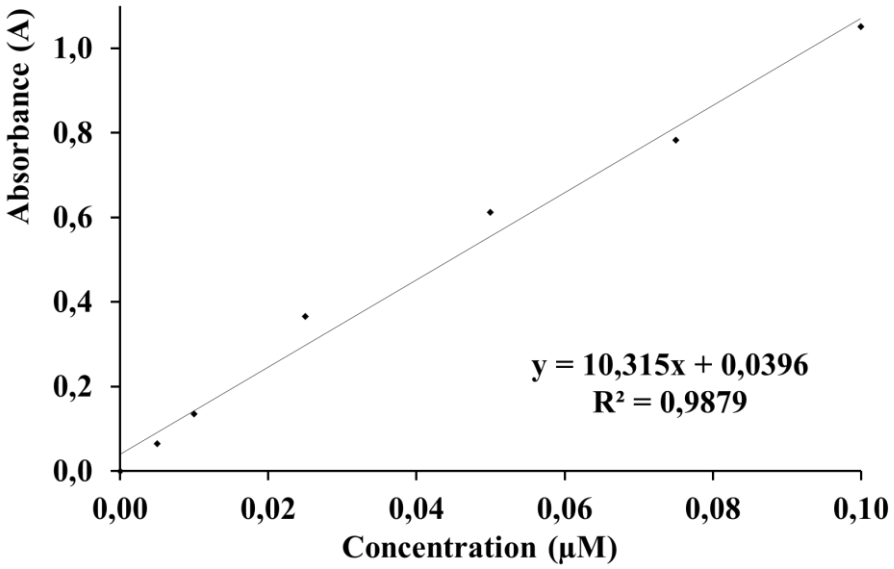

Appendix 1. Calibration curve for carbohydrates content.

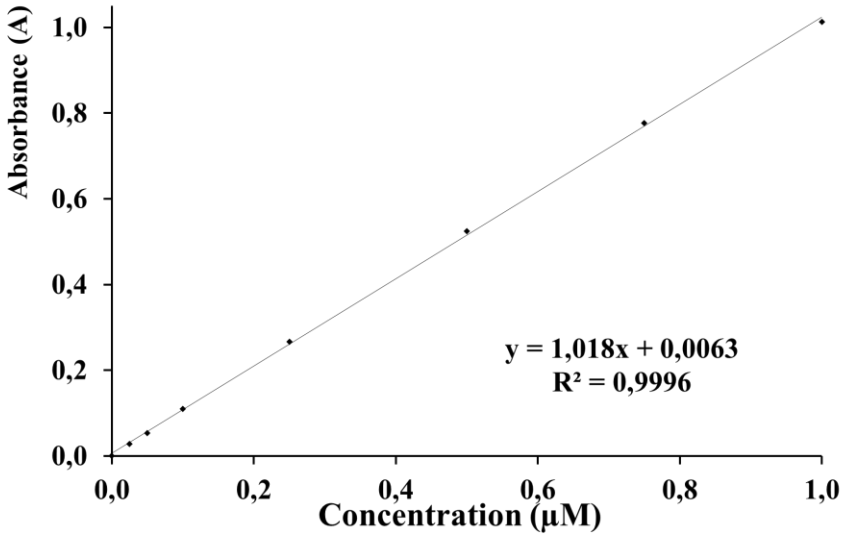

Appendix 2. Calibration curve for phenolic content.

Appendix 3. Size and PDI of all reactions tested in 24-well microplate.

Reaction	pH	TE (%) (vol/vol)	[AgNO3] (mM)	Z-Ave (d.nm)	PdI	ZP (mV)
1	8	0.25	1	412 ± 231	0.43 ± 0.17	-21.9 ± 1.9
2	9	0.25	1	235 ± 13	0.42 ± 0.03	0.2 ± 0.6
7	9	5	1	226 ± 28	0.51 ± 0.02	-21.9 ± 0.2
8	9	5	10	111 ± 1	0.24 ± 0	-36.8 ± 0.1
3	11	0.5	5	96 ± 8	0.37 ± 0.06	-0.3 ± 0.5
4	11	0.5	10	69 ± 2	0.46 ± 0.01	-0.6 ± 0.2
12	11	4	8	51 ± 2	0.88 ± 0.04	-21.7 ± 0.9
5	11	4.55	1	143 ± 1	0.40 ± 0	-10.3 ± 0.6
9	11	5	1	160 ± 3	0.32 ± 0.03	-30.9 ± 0.3
6	11	4.55	5	49 ± 0	0.48 ± 0	-28.5 ± 1.8
11	11	12.5	5	91 ± 2	0.36 ± 0.03	-40.5 ± 0.3
10	12	5	1	1714 ± 64	0.42 ± 0.02	-20.4 ± 0.2